PCCP

Phonon, thermal, and thermo-optical properties of halide perovskites

Journal:	*Physical Chemistry Chemical Physics*
Manuscript ID	CP-PER-08-2020-004426.R1
Article Type:	Perspective
Date Submitted by the Author:	25-Sep-2020

Complete List of Authors:	Handa, Taketo; Kyoto University, Institute for Chemical Research Yamada, Takumi; Kyoto University, Institute for Chemical Research Nagai, Masaya; Osaka University, Graduate School of Engineering Science Kanemitsu, Yoshihiko; Institute for Chemical Research,

Perspective Review
Physical Chemistry Chemical Physics

Phonon, thermal, and thermo-optical properties of halide perovskites

Taketo Handa,[a] Takumi Yamada,[a] Masaya Nagai[b] and Yoshihiko Kanemitsu*[a]

[a]Institute for Chemical Research, Kyoto University, Uji, Kyoto 611-0011, Japan
[b]Graduate School of Engineering Science, Osaka University, Toyonaka, Osaka 560-8531, Japan

Abstract

Metal halide perovskites are semiconductors with many fascinating characteristics and their widespread use in optoelectronic devices has been expected. High-quality thin films and single crystals can be fabricated by simple chemical solution processes and their fundamental electrical, optical, and thermal properties can be changed significantly by compositional substitution, in particular halogen ion. In this perspective, we provide an overview of phonon and thermal properties of metal halide perovskites, which play a decisive role in determining device performance. After a brief introduction to fundamental material properties, longitudinal-optical phonons and unusual thermal properties of metal halide perovskites are discussed. Remarkably, they possess very low thermal conductivities and very large thermal expansion coefficients despite their crystalline nature. In line with these discussions, we present optical properties governed by the strong electron–phonon interactions and the unusual thermal properties. By showing their unique thermo-optic responses and novel application examples, we highlight some aspects of the unusual thermal properties.

*E-mail: kanemitu@scl.kyoto-u.ac.jp

1 Introduction

Metal halide perovskites are promising materials for optoelectronic device applications and are being investigated intensively from fundamental viewpoints of physics and chemistry. Compared to conventional tetrahedral semiconductors with covalent bonds, such as Si and GaAs, halide perovskite semiconductors show complex but fascinating electrical and optical properties reflecting the structural diversities unique to the perovskite structure. Furthermore, in contrast to oxide perovskites that have been studied for a long time,[1–3] halide perovskites have an advantage that high-quality single crystals with very few defects can be fabricated by simple low-temperature solution processes. Therefore, they are widely expected to become cost-effective semiconductors for applications.[4–8]

A metal halide perovskite is described by the general chemical formula ABX_3 (A: monovalent cation, B: divalent metal ion, X: halogen ion). The cubic crystal structure of a lead halide perovskite is shown in Fig. 1a (drawn using VESTA[9]). The octahedra formed by BX_6 (shown in gray in the figure) mainly govern the electrical and optical properties. Stable and functional halide perovskites reported so far contain lead or tin as the B-site cation. In particular, lead halide perovskites exhibit excellent optical and transport properties, and many other features have been revealed.[4–8,10,11] The structural stability of the perovskite crystals is determined by the tolerance factor and the octahedral factor, which are defined by the ionic radii of the elements or molecules at A, B, and X sites.[12–14] Since a halide perovskite consists of the large metal cation at the B site, the A site needs to be occupied by organic molecules or inorganic Cs with large ionic radii to stabilize the crystal structure. Halide perovskites with organic molecules MA (CH_3NH_3) or FA [$CH(NH_2)_2$] at the A site are known as organic-inorganic hybrid perovskites, while those with inorganic Cs ion at the A site are known as all-inorganic halide perovskites. Substitution of the chemical species at each site allows for control over the materials properties. The intrinsic properties of halide perovskites can be elucidated by comparing samples with different compositions. The presence of a heavy metal element with a large ionic radius increases the bond length between the metal and halogen, which presumably leads to the soft lattice nature of this materials system and unusual thermal properties.

By taking advantages of the simple and low-cost fabrication and flexibility, their use in various devices is expected.[4–8] Solar cells are the application example demonstrated since the beginning of research.[15–17] Due to their excellent optoelectronic properties, further advances towards novel application schemes beyond solar cells have recently been discussed extensively, *e.g.*, photodetectors,[18,19] light-emitting diodes,[20] lasers,[21] light modulators,[22] nonlinear devices,[23–25] and quantum emitters.[26–29] In considering these applications, thermal properties of the material should be critical as they influence the stability and operation lifetime of devices. It has been reported that halide perovskites possess ultralow thermal conductivities and large thermal expansion coefficients.[30,31] Although these characteristics seem detrimental for practical implementation, new functionalities may also be realized if the impact of such thermal properties on other physical properties has been understood well. Because thermal properties are inherently related to phonons, phonon properties should be characterized as well. A deeper understanding of the phonon and thermal properties of these semiconductors is essential from both fundamental and application points of view.

In this perspective, we summarize characteristics of phonons and thermal behaviors in metal halide perovskite semiconductors. In addition to providing an overview of the relevant research results, the impact of the phonon and thermal properties on the optical responses is discussed based on our recent experimental results. We describe the broad photoluminescence (PL) spectrum due to the strong electron–phonon interaction and the unique temperature dependence of the optical properties resulting from the unusual thermal properties. Through comparisons between halide perovskites and conventional inorganic semiconductors, we highlight the characteristic thermo-optical responses of halide perovskites, followed by a brief description of their application examples. This perspective aims to shed more light on some positive aspects of the thermal properties by presenting the unique thermo-optical characteristics.

2 Fundamental material properties

In this section, we provide a brief introduction to the electronic structure near the band edge and also longitudinal optical (LO) phonons in metal halide perovskites. The former mainly governs the optoelectronic properties, while the latter influences the luminescence and charge transport properties via electron–phonon interactions.

2.1. Electronic band structure

Metal halide perovskites ABX_3 are semiconductors with direct band-to-band transitions and a large light absorption coefficient in the visible wavelength range.[32,33] They have a steep absorption spectrum below the band edge,[32] indicating few localized defect levels in the bandgap. In particular, lead halide perovskites exhibit a highly efficient luminescence.[34–37] The characteristic of their electronic band structure is that both the bottom of the conduction band and the top of the valence band are formed by antibonding orbitals (see Fig. 1b).[38–43] The small density of the defect levels within the bandgap has been attributed to this antibonding nature.[42,43] The conduction band mainly reflects the *p* orbital of Pb, and thus comprises the heavy and light electron bands and the spin split-off band due to the large spin-orbit interaction.[44] The separated split-off band constitutes the bottom of the conduction band, and thus there is no band degeneracy. Therefore, their optical properties near the band edge, including nonlinear optical properties, can be analyzed by a simple two-band model.[24,27]

A practically useful feature is that their bandgap energy E_g can be controlled by changing the element or molecule at each site.[45–48] This facilitates the fabrication of halide perovskite thin films with optimal bandgap energies for single-junction solar cells and tandem solar cells.[49–56] The elements or molecules typically used for the A site are FA, MA, and Cs, those for the B site are Pb and Sn, and those for the X site are Cl, Br, and I. So far, most investigations have been conducted on the combination of these elements and molecules.[57–59]

In order to compare the electronic structure and optical properties between the compounds with different compositions, it is necessary to study samples that are fabricated under a similar condition and with similar quality. In this respect, a recent experiment[60] showed the absolute energies of the top of the valence band and the bottom of the conduction band and the optical bandgap for typical 18 types of halide perovskites. Among them, the values of lead halide perovskites are summarized in Fig. 2. It is known that in tin halide perovskites,

the valence band maximum and the bandgap energy can be affected by the film quality and by oxygen and moisture.[61–64] In Fig. 2, it can be confirmed that by changing the halogen X the bandgap energy can be tuned over a wide range covering the whole visible wavelength region. Furthermore, the bandgap energy can be changed continuously by using a mixed-halide perovskite with more than one type of halogen (*e.g.* X = $I_{0.6}Br_{0.4}$).[65,66] Additionally, although the A-site cation has no direct influence on the electronic states near the band edge, it slightly alters the electronic structure through changing the lattice constant and tilting the PbX_6 octahedra.[60,67] In this way, a fine-tuning of the bandgap energy is possible. Since the compositions at A and X sites can be engineered independently, it is possible to manipulate the materials properties while maintaining the structural stability. Note that the variations in the reported values of E_g in the literature have their origin in the fact that the values can depend on the sample quality, measurement method, and analysis procedure.

The exciton binding energy is another important physical property that strongly depends on the halogen element.[68–70] The understanding and control of the exciton binding energy is essential because it governs the optical responses and charge transport properties. For example, $MAPbI_3$ is a prototypical lead halide perovskite, which has been intensively used in solar cells due to its relatively narrow bandgap energy of 1.61 eV.[32] The exciton binding energy in $MAPbI_3$ is smaller than 10 meV,[71,72] therefore, the excitons in $MAPbI_3$ dissociate into free electrons and free holes at room temperature.[34] In the wide-gap semiconductor $MAPbCl_3$, the exciton binding energy has a larger value of 41 meV, and thus stable excitons exist in this material at room temperature.[73]

Previously, the quality of tin halide perovskites was much poor compared to that of lead halide perovskites. The intrinsic optical and electronic properties of tin halide perovskites remain unclear. However, recent advances in fabrication processes have led to the fabrication of tin halide perovskite crystals and thin films with significantly improved quality,[74,75] which enabled high solar cell efficiencies comparable to those of lead halide perovskites in the initial stages of research.[76–78] Investigations using such high-quality tin halide perovskites will advance the understanding of their intrinsic properties,[79] which should be a target of future research. The following discussions in the present work mainly focus on the lead-based perovskites.

2.2. LO phonons

Here, we discuss LO phonons in lead halide perovskites, which play an important role in their optical properties and charge transport properties. In polar semiconductors including halide perovskites, the displacement of atoms due to the long-wavelength LO phonons induces the macroscopic polarization and uniform internal electric field. This results in the enhanced Coulomb interactions between the charge carriers and lattices.[80] Because the optical phonons originating from the PbX_6 cage appear in the low-frequency region,[81,82] the optical phonons influence their optical properties. Furthermore, when an organic molecular cation with a dipole is incorporated, the low-frequency vibration modes of the organic molecule can affect the phonons of the PbX_6 cage.[83,84] In Fig. 3, the measured absorption coefficient[85] and the calculated infrared activity[81,86] of the low-temperature phase of $MAPbI_3$ (at 10 K) are shown. Here, the phonons of the inorganic PbI_6 cage appear below 100 cm^{-1} and the vibration of the molecular A-site cation appears above 100 cm^{-1}.

These modes induce phonon–phonon scatterings and these scattering processes can determine the lifetimes of the phonons of the PbI_6 cage. The assignment of phonon modes that correspond to each phonon energy in halide perovskites has been discussed in ref. 81 and 86.

The LO phonon energy is the most fundamental parameter for discussion of the Fröhlich interaction, *i.e.*, the interaction between charge carriers and the Coulomb potential induced by the long-wavelength LO phonon. An accurate assessment of its value is necessary because the LO phonon energy strongly influences the polaron effect, linewidth of the PL spectrum, and carrier mobility. The values of the LO phonon energies have been characterized by several methods such as Raman spectroscopy,[86,87] terahertz (THz) spectroscopy,[88–91] and PL measurements.[92,93] However, even in $MAPbX_3$ that has been studied intensively, the variations in the reported values of the LO phonon energies are large. Below, we present the properties of the LO phonons as determined by THz spectroscopy measurements on high-quality single crystal samples.

The phonon properties have been investigated using $MAPbX_3$ single crystals and THz time-domain reflection spectroscopy in the frequency range below 230 cm^{-1}.[85] Three samples with different halogens (X = I, Br, and Cl) were measured to distinguish between the vibrations from the PbX_6 cage and other vibrations. The LO phonon was directly characterized from the spectrum of the energy loss function $Im[-1/\epsilon]$ that represents the longitudinal excitation.[94] In Fig. 4a, the $Im[-1/\epsilon]$ spectrum of $MAPbI_3$ is shown, which was obtained from the measured dielectric constant of the $MAPbI_3$ single crystal. The results for other halide perovskites can be found in ref. 85. At 300 K, the LO phonon in $MAPbI_3$ appears at approximately 130 cm^{-1} (it is located at 160 cm^{-1} in $MAPbBr_3$[85]). This result is almost the same as the other report based on the Fourier transform infrared measurements.[90] Note that due to the presence of the heavy Pb atom in lead halide perovskites, their phonon frequencies are much lower than those in conventional inorganic semiconductors (*e.g.*, the LO phonon frequency is 292 cm^{-1} for GaAs[80]). This can have a large influence on the electron-hole recombination and the intraband relaxation mechanisms.[95]

The LO phonon frequency increases as the halogen X is changed from I to Br to Cl (from heavier to light atoms), which shows that the LO phonon mainly originates from the PbX_6 cage.[85,96] Because the real part of the dielectric constant is close to zero at the frequency of LO phonon,[80] the spectrum of $Im[-1/\epsilon]$ can be modulated by a very small dielectric component. Indeed, in Fig. 4a, the LO phonon peak is split into two peaks located at 110 and 165 cm^{-1} at low temperatures.

A highly interesting feature is that the averaged energy of the split LO phonons at low temperatures is constant independent of the temperature (see Fig. 4b; black squares). While the LO phonon spectrum changes significantly with temperature, its averaged frequency stays at 131 cm^{-1} in $MAPbI_3$ for wide temperature range. This means that the nature of the LO phonon stays essentially unchanged below and above the phase transition temperature and its coupling with charge carriers via the Fröhlich interaction does not change much. This will be examined further in Section 3.1 in line with the discussion of the temperature dependent PL linewidth.

As discussed above, the bandgap energy changes strongly with the halogen X, but it is also modulated slightly by the A-site cation. In the same way, it is expected that the LO phonon spectra are also changed by the A-site cation. The lifetime of the LO phonon is generally determined by its coupling with acoustic

phonons,[97] and thus the A-site cation can influence the energy relaxation of carriers via phonon–phonon scattering. A detailed discussion is provided in Section 3.2.

3 Electron–phonon interactions and their impact on the optical spectra and carrier dynamics

In Section 2, we briefly described the fundamental electronic structure and the phonon properties. In the present section, we discuss how the PL spectra and carrier relaxation processes are influenced by phonons via electron–phonon interactions. Metal halide perovskites possess highly polar properties and show a large splitting between the LO phonon and the transverse optical phonon,[90] which suggests that strong electron–phonon interactions occur. Note that halide perovskites are materials that a deep understanding of electron–phonon interactions is important.

3.1 PL linewidth

In polar semiconductors, the linewidth of the PL spectrum is dominated by the electron–LO phonon interaction via the Fröhlich interaction. The contributions of impurities and the acoustic phonon cannot be neglected at low temperatures. Fig. 4c shows the temperature dependence of the PL linewidth obtained from the $MAPbI_3$ single crystal.[85] Although the PL spectral shape changes strongly at the phase-transition point, the linewidth of the PL spectrum exhibits no abrupt change. The temperature dependence of the PL linewidth can be well explained for the whole temperature range by using the single effective LO phonon energy shown in Fig. 4b. This result shows that the effective LO phonon frequency does not change with temperature and the strength of the electron–phonon interaction is almost independent of the crystal structure; this is in agreement with the conclusion derived from Fig. 4b. Similar results have also been reported for $MAPbBr_3$.[85]

Fig. 5a shows the room-temperature PL spectra of a $MAPbI_3$ thin film under resonant excitation.[98] The sharp lines in the figure represent the scattering of the excitation light, showing that the excitation energy was varied from well above to slightly below the PL peak energy. This result clearly demonstrates that the broad spectrum of $MAPbI_3$ does not change even when excited within the PL band. In other words, the broad PL reflects the thermal distribution of carriers[99] and the linewidth is determined by strong electron–phonon interactions. This is consistent with the result in Fig. 4c that the temperature dependence of the PL linewidth is determined by the electron–LO phonon interaction. Comparable PL characteristics were also obtained for a $MASnI_3$ thin film as shown in Fig. 5b, which is an important observation for the development of lead-free materials for optoelectronic device applications.[62,100] In addition to these studies on thin films and single crystals, recent single-dot spectroscopy measurements on highly luminescent halide perovskite nanocrystals have been revealing the impact of the electron-phonon interaction and the A-site cation on the PL spectrum and PL dynamics.[101–104]

Another remarkable result in Fig. 5a is that anti-Stokes PL is clearly observed. Here, the anti-Stokes PL refers to the emission with photon energies higher than the excitation photon energy. This efficient anti-Stokes PL is likely to occur via the absorption of phonons in the material. Therefore, if the material has a high external PL quantum efficiency, the removal of thermal vibrations (phonons) through the anti-Stokes process can enable a decrease in the material's lattice temperature, *i.e.*, laser cooling.[98,105] The PL excitation

measurement has been employed to investigate the anti-Stokes PL efficiency and the cooling gain in the iodide perovskite $MAPbI_3$, and their relation to photon recycling has been discussed.[98] Furthermore, it was shown that the anti-Stokes PL in two-dimensional perovskite $(C_6H_5C_2H_4NH_3)_2PbI_4$ is dominated by free excitons in contrast to the free-carrier-dominated PL in the three-dimensional $MAPbI_3$.[106]

The PL spectral shape is also well described using the absorption spectrum and such analysis allows for the further discussion on the electron–phonon interactions. In a semiconductor at thermal equilibrium, the spontaneous emission rate and the absorption probability at a given photon energy are connected via the van Roosbroeck–Shockley relation.[107] If the exposure time is set sufficiently long, the PL spectrum measurement can be used to accurately evaluate the spectral shape of the PL tail where the PL intensity is very small. By using the obtained PL spectrum and the van Roosbroeck–Shockley relation, it becomes possible to accurately characterize the exponential shape that appears in the absorption tail region below the bandgap, *i.e.*, the Urbach tail.[108–110] Based on the expression given in the literature,[108] the PL spectrum $I_{\mathrm{PL}}(E,T)$ can be written using the absorption spectrum $\alpha(E,T)$:

$$I_{\mathrm{PL}}(E,T) \propto \frac{\alpha(E,T)E^2}{\exp\left[(E-\Delta\mu)/k_{\mathrm{B}}T\right]-1} \propto \alpha(E,T)E^2\exp\left(-E/k_{\mathrm{B}}T\right). \quad (1)$$

Here, E represents the photon energy, k_{B} represents the Boltzmann constant, T represents the temperature, and $\Delta\mu$ represents the difference between the electron and hole quasi-Fermi levels. Because the PL spectra discussed here were obtained under weak excitation conditions, $E-\Delta\mu \gg k_{\mathrm{B}}T$ is considered fulfilled and thus the approximation for the second line in eqn (1) holds.

Fig. 5c and 5d show the PL as well as absorption spectra of the $MAPbI_3$ and $MASnI_3$ thin films at room temperature. Both the lead and tin iodide perovskites exhibit a sharp absorption edge and their PL peak is located near the absorption onset energy, *i.e.*, there exists almost no luminescence Stokes shift. The small luminescence Stokes shift in conjunction with the high PL quantum yield, especially in the lead-based perovskite, would result in the repeated cycles of photon emission and reabsorption: efficient photon recycling.[111] This is a beneficial characteristic when this material is used in photovoltaic devices.[112–119] The spontaneous emission spectra calculated from eqn (1) are indicated in Fig. 5c and 5d with the black circles. For this calculation, a temperature of T = 300 K and a constant refractive index are assumed. The experimental data of the PL spectrum agrees well with the spontaneous emission spectrum calculated using eqn (1) and the experimental absorption spectrum. This confirms that the thermal equilibrium of carriers is well established and the PL spectrum is directly related to the absorption spectrum.

Based on the relation between PL and absorption, the small absorption coefficient in the sub-bandgap region and the Urbach energy E_{U} can be evaluated by analyzing the tail of the PL spectrum. Note that the Urbach energy is a very important material parameter from both fundamental and practical viewpoints because it is not only the measure of a voltage drop in a photovoltaic device,[120–123] but also it indicates the strength of electron–phonon interactions in a material.[124] The values of E_{U} = 13 meV for $MAPbI_3$ and E_{U} = 12 meV for $MASnI_3$ were obtained from the analysis of the PL spectra with eqn (1). These values are almost

the same as those obtained for high-quality perovskite samples in other reports.[125–127] These Urbach energies are relatively small when we consider that both samples are polycrystalline thin films fabricated by a low-temperature solution process. This result verifies that there are almost no defect levels near the band edge. Since the small E_U is an essential property to realize solar cells with high open-circuit voltages,[120–123] these results show that the fundamental absorption properties of the metal halide perovskites are suitable for application in photovoltaic devices.

3.2 Hot-carrier cooling dynamics

Electron–phonon interactions play an important role in the photoexcited carrier dynamics in metal halide perovskites. In particular, recent reports have shown that the intraband relaxation of carriers with excess energies is remarkably slow in halide perovskites compared to that in conventional inorganic semiconductors (see Fig. 6a).[128–133] The long lifetimes of hot carriers in halide perovskites attract much attention because they potentially enable highly efficient hot-carrier solar cells whose power conversion efficiency can exceed the Shockley-Queisser limit.[134–137] The understanding of the hot-carrier dynamics is also important in terms of the application to optical amplification and light emission because the manipulation of hot-carrier states, including hot excitons and hot biexcitons in halide perovskite nanocrystals, can control the optical gain behavior.[138–141]

With respect to hot-carrier cooling processes in a lead iodide perovskite, a systematic experimental result that reveals a hot-phonon bottleneck effect has been reported.[128] As shown in Fig. 6b, a characteristic elongation of the hot carrier relaxation time was observed in a $MAPbI_3$ thin film when the initial carrier density exceeds ~10^{18} cm^{-3}. The energy relaxation time constant was several tens of picoseconds, which is three orders of magnitude longer than the value observed in bulk GaAs under the similar excitation condition. Note that, at early times just after the excitation, the energy loss rate (corresponding to the slope of the cooling curve in Fig. 6b) is almost independent of the carrier density, where the efficient emission of LO phonons determines the energy loss rate. A large decrease in the energy loss rate is observed after the carriers lose much of their kinetic energies, which results in the overall slow relaxation. Such slow hot-carrier relaxation has been observed only when a sufficiently large excess energy is provided by photoexcitation as shown below.

In Fig. 6c, we summarized the reported hot-carrier relaxation time constants for different lead iodide perovskite ($APbI_3$; A = MA, FA, and Cs) thin films. This figure is based on the reports discussing the electronic temperature by means of the transient absorption technique,[128,129,142–144] and the relaxation time shown here is defined at which the electronic temperature cools down to 600 K.[131] It is shown in Fig. 6c that the relaxation time constant at high excitation densities becomes larger when the photoexcited carriers have a large excess energy. A similar trend can be seen for the hybrid and all-inorganic lead iodide perovskites.

The slower hot-carrier relaxation at high excitation densities in the lead iodide perovskites is similar to the hot-carrier dynamics in III–V quantum wells.[145] In the latter, the slower carrier relaxation at high excitation conditions has been interpreted as a hot-phonon bottleneck effect: a large population of hot carriers generates many nonequilibrium LO phonons and these hot phonons can be reabsorbed by electrons and keep them

hot.[146] In metal halide perovskites, several models have been proposed to explain the origin of the hot-phonon bottleneck and under intense discussion: a large phononic gap between the effective LO phonon frequency and the frequency of the zone-boundary acoustic phonon,[142] an efficient acoustic-to-optical phonon up-conversion due to a large overlap between acoustic and optical phonon modes,[143] and a very low thermal conductivity of these materials.[147] Additionally, attention has been paid to how the relaxation process is affected by the modification in the phonon density of states upon the A-site cation substitution, which stimulates both experimental and theoretical investigations of bulk and nanocrystal samples.[148,149] Note that for a comprehensive discussion of carrier dynamics in nanocrystal samples, a detailed understanding of a tion, which is formed by one exciton and a bound electron or hole, is necessary.[150] This is because in halide perovskite nanocrystals the trions can be generated even under weak excitation conditions[27,28] and they have a large impact on their carrier dynamics.[150,151]

Moreover, even for weak excitation conditions of initial carrier densities below 10^{18} cm^{-3}, unique slow hot-carrier relaxation has been reported. In hybrid perovskites $FAPbBr_3$, $MAPbBr_3$, and $MAPbI_3$, hot-carrier PL signals with exceptionally long time constants of several hundreds of picoseconds have been observed.[83,152] The striking difference in contrast to the hot-phonon bottleneck under strong excitation is that the effective electron temperature derived from the initial PL spectrum decreases with increasing excitation fluence (see Fig. 6d).[152] As the origin of this behavior, the suppression of the electron–LO phonon scattering due to a dynamic screening of the molecular cation has been proposed.[83,153] This model is supported by the experimental results that the hot-carrier PL observed in $MAPbBr_3$ and $FAPbBr_3$ is not observed in $CsPbBr_3$ with no organic molecule, and the hot-carrier PL of $MAPbBr_3$ disappears in the low-temperature phase where the rotation of the organic MA molecule freezes.[83] Similar PL results have been reported in another publication.[154]

Together with the abovementioned long relaxation time, the long-range transport of hot carriers has also been reported for the lead iodide perovskite $MAPbI_3$.[155] Therefore, lead halide perovskites have several highly promising properties for hot-carrier solar cells. Additionally, hot-carrier PL with a long time constant was also observed in a tin iodide perovskite,[156] which should be important for the elucidation of the fundamental mechanisms and also for the development of lead-free materials.

There still remain unsolved questions regarding the hot-carrier relaxation dynamics, but it seems reasonable to consider that the unique phonon modes, electron–phonon interactions, and strong anharmonicity should be of high relevance. Note that, as can be seen in Fig. 6c, there exist variations between the reported hot-carrier relaxation time constants in the literature. The sample fabrication procedures have been improved and high-quality samples can be obtained recently, and thus further investigations on such high-quality samples will enable more comprehensive understandings of the hot-carrier dynamics. In addition, most investigations to date have been performed under very strong excitation conditions that cannot be achieved even in concentrator photovoltaics. Thus, it will be important to study the electron–electron scattering and the hot-carrier relaxation under weak photoexcitation close to the actual operating conditions for further development of perovskite-based solar cells.[146,157]

4 Thermal and thermo-optical properties

For the practical implementation of metal halide perovskites, understanding of their thermal properties should be of great importance. In particular, the thermal expansion and thermal conduction play a critical role for device performance and arise from the anharmonic effect of phonons. Considering the phonon characteristics discussed above, halide perovskites can exhibit rather unconventional thermal properties. The first half of this section presents their unconventional thermal properties, and in the second half we will show that metal halide perovskites are totally unique materials with unusual thermo-optical properties.

4.1 Thermal conductivity and thermal expansion coefficient

The thermal conduction is a phenomenon that is governed by the phonon–phonon scattering and the phonon mean free path. In metal halide perovskites featuring characteristic structural softness,[158,159] the thermal properties including the thermal conductivity have been the subject of intense research.[160] The exceptionally low thermal conductivity of organic–inorganic hybrid perovskites was first reported in 2014.[30] The temperature dependence of the thermal conductivity was measured for a $MAPbI_3$ single crystal and a polycrystalline thin film. As shown in Fig. 7a, both samples have a low thermal conductivity of ~0.5 W m^{-1} K^{-1} at room temperature. This value is significantly low among crystalline solids and we will present a thorough comparison later. In Fig. 7a, no significant difference is found in the absolute values and the temperature dependence between the single crystal and thin film. The low thermal conductivity is attributed to the small group velocity and the short lifetime of phonons.[30,161] Theoretical considerations have pointed out that the strong interaction between the rotation of the MA molecule and the low-frequency phonons of the PbI_6 cage can lead to the low thermal conductivity.[162]

As is the case for the optical properties discussed in the preceding section, the impact of the organic molecular cation on the thermal conductivity has also been a topic of interest. It was reported that the all-inorganic perovskites $CsPbI_3$, $CsPbBr_3$, and $CsSnI_3$ have low thermal conductivities of about 0.4 W m^{-1} K^{-1} at room temperature, *i.e.*, almost same as that of the organic–inorganic hybrid perovskite.[163] The thermal conductivity in halide perovskites at around room temperature is thus almost independent of the type of the A-site cation.[163,164] The role of the A-site cation can be seen at low temperatures.

In organic–inorganic hybrid perovskites, the thermal conductivity at room temperature strongly depends on the halogen atom. As was mentioned in Section 2, the electronic structure and the LO phonon frequency also depend strongly on the halogen. These consequences are attributed to the same reason: the strength of the Pb–X bond that depends on the ionic radius. In Fig. 7b, the experimental results on different halogens are shown.[165] For example, in the case of chloride, the ionic radius is small and the density is relatively large, which lead to the larger strength of the Pb–Cl bond and the hydrogen bond. In Fig. 7b, the thermal conductivity k is plotted as a function of $C_{a\text{-}cubic}\bar{v_s}/3$, where $C_{a\text{-}cubic}$ is the volumetric heat capacity of acoustic phonons based on a cubic unit cell and $\bar{v_s}$ is an average sound speed. The dashed line is a linear fit for $MAPbX_3$. The slope of the fitting curve gives the average acoustic phonon mean free path $\bar{\Lambda a} = 4.3 \pm 1.1$ nm. The nonzero y-intercept indicates that optical phonons also contribute to the thermal conductivity.[165] Theoretical analysis suggested that the mean free path of a large part of the phonons responsible for thermal

conduction is less than 100 nm.[165] Consequently, as long as the grain size is larger than about 100 nm, the scattering at the grain boundary does not affect the conductivity; therefore, similar results can be obtained for single crystals and polycrystalline thin films (Fig. 7a). Compatible results were obtained with theoretical calculations and neutron scattering showing a small acoustic-phonon lifetime[86,161,166] and a small phonon group velocity due to the small elastic modulus that corresponds to the structural softness.[159]

The thermal conductivity can also be determined by measuring the transient refractive index change. This is based on the evaluation of the optical phase shift resulting from the temperature-induced refractive index change by combining a time-resolved optical interferometer[22] and optical beam-induced heating (Fig. 8a). During optical excitation, the excitation laser beam behaves as a heat source and this leads to a gradual temperature rise around the beam spot whose temporal evolution reflects the thermal conductivity of a material.[167] By measuring the temporal evolution of the resulting refractive index change as the optical phase shift of the probe light, the thermal conductivity was determined in a contactless manner. In Fig. 8b, the optical phase of the probe light transmitted through a $MAPbCl_3$ single crystal is presented, showing that the optical phase advances under optical excitation.[168] In Fig. 8c, it is shown that this phase shift occurs slowly with a time constant of milliseconds during the optical excitation. By performing an analysis based on a model accounting for the photo-induced temperature rise and the thermal conduction, the thermal conductivity of $MAPbCl_3$ was determined to be 0.46 W m^{-1} K^{-1}, in agreement with the previously reported values.

The thermal expansion is another important property that affects the device degradation and performance. It has been reported that the thermal expansion coefficients of halide perovskites are much larger than those of conventional inorganic semiconductors.[31,158,169] In ref. 170, it is pointed out that metal halide perovskites are semiconductors that possess a very low thermal conductivity and a very large thermal expansion coefficient. Fig. 9 shows the relation between these two thermophysical properties for a wide range of materials. The values used in this figure were obtained from the literature: $MAPbX_3$ with X = I, Br, and Cl from ref. 170, $CsPbI_3$ from ref. 163,171, other inorganic solids from ref. 172, and polymers and liquids from ref. 173.

In Fig. 9, the group IV semiconductors with covalent bonding and the III–V semiconductors with slightly ionic bonding are located at the lower right corner of the figure. The more ionic solids are located at the upper left side. Among inorganic solids, halide perovskites are at the most upper left position. This characteristic is even more pronounced than in the soft and insulating ionic crystals (group I–VII materials, such as NaCl). Halide perovskites show thermal properties that resemble those of organic polymers or even liquids. This characteristic is confirmed for both hybrid and all-inorganic halide perovskites (see Fig. 9), which indicates that the inorganic PbX_6 cage dominates the thermal properties. A similar behavior is observed when Pb is substituted for Sn.[174] Additionally, it was recently reported that $FAPbI_3$ exhibits a large negative thermal expansion coefficient at low temperatures near the phase transition point.[175]

Since both the thermal conduction and thermal expansion are generally governed by the anharmonic interaction of phonons, the above characteristics indicate the strong phonon anharmonicity in halide perovskites. The presence of the heavy elements with large ionic radii leads to a long bond length between

the metal and halogen, which presumably gives rise to the soft lattice nature and the unique thermal properties of this material system. Thermal properties can depend on the sample quality, thus systematic measurements for high-quality samples will be helpful for more comprehensive understanding.

4.2 Temperature dependence of optical properties

As presented in the above section, there has been progress in understanding the thermal properties of halide perovskites. The consequences and implications of these findings can be easily envisioned, *i.e.*, the low thermal conductivity can lead to a temperature rise of an operating device and cause a stability issue and the large thermal expansion can gives rise to thermal strain and stress. These aspects are indeed important in considering actual implementation of halide perovskites, while we can also expect that these unusual properties can be utilized in a positive way. For example, the low thermal conductivity will open a way for thermoelectric application.[176,177] Here, we should bear in mind that the most important characteristic of halide perovskites is that they possess excellent optical properties. In this respect, increasing attention has been paid to the temperature dependence of their optical properties.

Recent studies have discovered intriguing thermo-optical responses and these have been further utilized in novel applications.[168,178–180] Here, we present the unique temperature dependence of refractive index observed in halide perovskites.[168] The refractive index is a fundamental optical constant for the design of photonic devices and its change upon temperature variation should be understood for stable device operation.[181] For the following discussion, note that conventional inorganic semiconductors exhibit an increase in the refractive index as the temperature increases, *i.e.*, they possess a positive thermo-optic coefficient.[182]

In Fig. 8b and 8c in the previous section, the optical phase of the transmitted light advances due to the photo-induced temperature rise. This means that the temperature rise results in a reduction in the optical path length, suggesting that halide perovskites are peculiar materials where the refractive index decreases with a temperature increase. This result was verified by independent measurements of incident-angle dependence of the surface reflection, clearly showing that the halide perovskite $MAPbCl_3$ possesses a negative thermo-optic coefficient.[168] For comparison with other materials, the normalized thermo-optic coefficient and the thermal conductivity of various materials are summarized in Fig. 10a. The halide perovskite $MAPbCl_3$ exhibits a negative thermo-optic coefficient, which is hardly observed in conventional inorganic semiconductors. We can confirm that halide perovskites have a characteristic that rather resembles that of organic materials or liquids.

The low thermal conductivity of halide perovskites leads to a large increase in the local temperature in the vicinity of the excitation laser spot. This facilitates a contactless and efficient modulation of material properties. Fig. 10b summarizes the expected changes of the refractive indices due to the laser light excitation that are calculated for various materials using the thermo-optic coefficients and the temperature increase caused by a given absorbed power of light (here, 20 mW).[168] Obviously, the halide perovskite exhibits an exceptionally large thermo-optic response. In fact, lead chalcogenides also show a negative thermo-optic coefficient and a large refractive index change; however, their narrow bandgap energy located at the mid-

infrared region makes them unsuitable for applications in the near-infrared and visible regions.[80] Halide perovskites are high-quality semiconductor materials that provide a combination of high transparency and unique thermo-optic properties in the visible range.

Recently, it was shown that the negative thermo-optic coefficient predominantly originates from the large thermal expansion coefficient of halide perovskites.[183.] According to the Lorentz oscillator model, the temperature dependence of the refractive index at energies below the fundamental absorption edge can be expressed in terms of (i) the thermal shift of the resonance energy and (ii) the change of the valence electron density due to thermal expansion.[184,185] The contributions of the energy shift and the thermal expansion to the thermo-optic coefficient can be clearly understood by a plot as in Fig. 11.[183] This figure shows that, in semiconductors except the halide perovskite, the magnitude and the sign of the normalized thermo-optic coefficient are determined by the shift of the absorption-edge energy, *i.e.*, they lie on the gray linear line. Because the thermal expansion coefficient is small in these conventional semiconductors,[186,187] the thermal shift of the resonance energy dominates the thermo-optic coefficient. On the other hand, the halide perovskite $MAPbCl_3$ is far off the gray line; it exhibits a large negative thermo-optic coefficient despite a small absorption-edge shift. Such a characteristic is caused by a large decrease in the valence electron density with increasing temperature owing to the large thermal expansion.[183] The negative thermo-optic coefficient is thus an interesting property that reflects the electronic structure and lattice properties of halide perovskites. It is expected that the large change in the valence electron density with temperature affects not only the refractive index but also many optical responses.

Finally, we briefly describe several other temperature-dependent optical responses. In metal halide perovskites, a blueshift of the absorption edge and PL peak energies has been observed,[71,188] which is opposite to the redshift usually observed in conventional semiconductors.[80] The ultraviolet photoemission spectroscopy and theoretical calculations have shown that the blueshift with increasing temperature can be understood in terms of the orbital nature of their valence band.[178,189] Because the valence band maximum of metal halide perovskites is formed by a strong mixing of the Pb and halogen orbitals (Fig. 1b), the increase in the inter-atom distance due to the thermal expansion leads to the large lowering of the valence band maximum, resulting in the blueshift. The importance of the electron–phonon interactions has also been pointed out.[190]

Furthermore, it was reported that perovskite-like materials with low dimensionality exhibit a PL lifetime that is highly sensitive to temperature. This characteristic enabled remote thermal imaging with high resolution.[180] The application to smart photovoltaic windows has also been demonstrated, using the large changes in the bandgap energy followed by the sequential phase transitions in halide perovskites.[179] As such, the unique thermal changes of the optical properties can realize completely new optical functionalities. Also, using the negative thermo-optic coefficient of $MAPbCl_3$, the passive compensation of the thermally-induced optical phase shift occurring in a ZnSe crystal was demonstrated.[168] Moreover, based on the calculation that predicts the efficient thermo-optic modulation characteristics as in Fig. 10b, the polarization control of visible light was demonstrated using the optical phase modulation (Fig. 12).[168] Considering the unique thermal properties of halide perovskites, we can expect that further interesting thermo-optical properties are waiting

to be discovered. These will enable novel applications that can only be realized with halide perovskite semiconductors.

5 Conclusions

This perspective has presented the recent progress in understanding the phonon and thermal properties and their impact on the optical responses in metal halide perovskites. Much discussion has been devoted to the fundamental optical properties based on our recent results, with showing their application examples. Metal halide perovskites have debuted as photovoltaic materials that provide high power conversion efficiencies but are simple to fabricate, thus, they have been promising materials for large-area implementation. Following thorough investigations have also shown their high potential as luminescent materials and nonlinear optics materials. Taking $MAPbX_3$ as a representative example, we have described the technically relevant features, such as the anti-Stokes PL, the thermal properties, and the temperature dependence of the refractive index. Remarkably, they possess exceptionally small thermal conductivities and large thermal expansion coefficients, which lead to unique thermo-optical responses. In the present work, attempts have been made to increase the awareness of the fact that the unusual thermal properties are not only problematic in applications, but also can enable novel applications, *e.g.*, the optical phase compensation and the thermo-optic modulation. Further comprehensive work on their fundamental properties will enable the discovery of new phenomena and the utilization in novel applications that are not available in conventional inorganic or organic semiconductors.

Conflicts of interest

There are no conflicts to declare.

Acknowledgements

The authors would like to thank many colleagues for their contributions and discussions. In particular, the authors gratefully acknowledge Professor A. Wakamiya, Professor Y. Yamada, and Dr. Hirokazu Tahara for helpful discussions. Part of this work was supported by JST-CREST (Grant No. JPMJCR16N3).

References

1 J. G. Bednorz and K. A. Müller, Perovskite-type oxides—The new approach to high-T_c superconductivity, *Rev. Mod. Phys.*, 1988, **60**, 585–600.

2 M. Imada, A. Fujimori and Y. Tokura, Metal-insulator transitions, *Rev. Mod. Phys.*, 1998, **70**, 1039–1263.

3 Y. Kanemitsu and Y. Yamada, Band-Edge Luminescence from Oxide and Halide Perovskite Semiconductors, *Chem. Asian J.*, 2020, **15**, 709–717.

4 S. D. Stranks and H. J. Snaith, Metal-halide perovskites for photovoltaic and light-emitting devices, *Nat. Nanotechnol.*, 2015, **10**, 391–402.

5 B. R. Sutherland and E. H. Sargent, Perovskite photonic sources, *Nat. Photonics*, 2016, **10**, 295–302.

6 Y. Kanemitsu, Luminescence spectroscopy of lead-halide perovskites: materials properties and application as photovoltaic devices, *J. Mater. Chem. C*, 2017, **5**, 3427–3437.

7 Q. A. Akkerman, G. Rainò, M. V. Kovalenko and L. Manna, Genesis, challenges and opportunities for colloidal lead halide perovskite nanocrystals, *Nat. Mater.*, 2018, **17**, 394–405.

8 Y. Kanemitsu and T. Handa, Photophysics of metal halide perovskites: From materials to devices, *Jpn. J. Appl. Phys.*, 2018, **57**, 090101.

9 K. Momma and F. Izumi, VESTA 3 for three-dimensional visualization of crystal, volumetric and morphology data, *J. Appl. Crystallogr.*, 2011, **44**, 1272–1276.

10 L. M. Herz, Charge-Carrier Dynamics in Organic-Inorganic Metal Halide Perovskites, *Annu. Rev. Phys. Chem.*, 2016, **67**, 65–89.

11 K. Miyata, T. L. Atallah and X.-Y. Zhu, Lead halide perovskites: Crystal-liquid duality, phonon glass electron crystals, and large polaron formation, *Sci. Adv.*, 2017, **3**, e1701469.

12 V. M. Goldschmidt, Die Gesetze der Krystallochemie, *Naturwissenschaften*, 1926, **14**, 477–485.

13 C. Li, K. C. K. Soh and P. Wu, Formability of ABO_3 perovskites, *J. Alloys Compd.*, 2004, **372**, 40–48.

14 C. Li, X. Lu, W. Ding, L. Feng, Y. Gao and Z. Guo, Formability of ABX_3 (X = F, Cl, Br, I) halide perovskites, *Acta Crystallogr. Sect. B Struct. Sci.*, 2008, **64**, 702–707.

15 A. Kojima, K. Teshima, Y. Shirai and T. Miyasaka, Organometal Halide Perovskites as Visible-Light Sensitizers for Photovoltaic Cells, *J. Am. Chem. Soc.*, 2009, **131**, 6050–6051.

16 M. M. Lee, J. Teuscher, T. Miyasaka, T. N. Murakami and H. J. Snaith, Efficient Hybrid Solar Cells Based on Meso-Superstructured Organometal Halide Perovskites, *Science*, 2012, **338**, 643–647.

17 H.-S. Kim, C.-R. Lee, J.-H. Im, K.-B. Lee, T. Moehl, A. Marchioro, S.-J. Moon, R. Humphry-Baker, J.-H. Yum, J. E. Moser, M. Grätzel and N.-G. Park, Lead Iodide Perovskite Sensitized All-Solid-State Submicron Thin Film Mesoscopic Solar Cell with Efficiency Exceeding 9%, *Sci. Rep.*, 2012, **2**, 591.

18 L. Dou, Y. (Micheal) Yang, J. You, Z. Hong, W.-H. Chang, G. Li and Y. Yang, Solution-processed hybrid perovskite photodetectors with high detectivity, *Nat. Commun.*, 2014, **5**, 5404.

19 S. Yakunin, M. Sytnyk, D. Kriegner, S. Shrestha, M. Richter, G. J. Matt, H. Azimi, C. J. Brabec, J. Stangl, M. V. Kovalenko and W. Heiss, Detection of X-ray photons by solution-processed lead halide perovskites, *Nat. Photonics*, 2015, **9**, 444–449.

20 Z.-K. Tan, R. S. Moghaddam, M. L. Lai, P. Docampo, R. Higler, F. Deschler, M. Price, A. Sadhanala, L. M. Pazos, D. Credgington, F. Hanusch, T. Bein, H. J. Snaith and R. H. Friend, Bright light-emitting diodes based on organometal halide perovskite, *Nat. Nanotechnol.*, 2014, **9**, 687–692.

21 G. Xing, N. Mathews, S. S. Lim, N. Yantara, X. Liu, D. Sabba, M. Grätzel, S. Mhaisalkar and T. C. Sum, Low-temperature solution-processed wavelength-tunable perovskites for lasing, *Nat. Mater.*, 2014, **13**, 476–480.

22 H. Tahara, T. Aharen, A. Wakamiya and Y. Kanemitsu, Photorefractive Effect in Organic-Inorganic Hybrid Perovskites and Its Application to Optical Phase Shifter, *Adv. Opt. Mater.*, 2018, **6**, 1701366.

23 H. Hirori, P. Xia, Y. Shinohara, T. Otobe, Y. Sanari, H. Tahara, N. Ishii, J. Itatani, K. L. Ishikawa, T.

Aharen, M. Ozaki, A. Wakamiya and Y. Kanemitsu, High-order harmonic generation from hybrid organic–inorganic perovskite thin films, *APL Mater.*, 2019, **7**, 041107.

24 K. Ohara, T. Yamada, H. Tahara, T. Aharen, H. Hirori, H. Suzuura and Y. Kanemitsu, Excitonic enhancement of optical nonlinearities in perovskite $CH_3NH_3PbCl_3$ single crystals, *Phys. Rev. Mater.*, 2019, **3**, 111601(R).

25 Y. Sanari, H. Hirori, T. Aharen, H. Tahara, Y. Shinohara, K. L. Ishikawa, T. Otobe, P. Xia, N. Ishii, J. Itatani, S. A. Sato and Y. Kanemitsu, Role of virtual band population for high harmonic generation in solids, *Phys. Rev. B*, 2020, **102**, 041125(R).

26 Y.-S. Park, S. Guo, N. S. Makarov and V. I. Klimov, Room Temperature Single-Photon Emission from Individual Perovskite Quantum Dots, *ACS Nano*, 2015, **9**, 10386–10393.

27 N. S. Makarov, S. Guo, O. Isaienko, W. Liu, I. Robel and V. I. Klimov, Spectral and Dynamical Properties of Single Excitons, Biexcitons, and Trions in Cesium–Lead-Halide Perovskite Quantum Dots, *Nano Lett.*, 2016, **16**, 2349–2362.

28 N. Yarita, H. Tahara, T. Ihara, T. Kawawaki, R. Sato, M. Saruyama, T. Teranishi and Y. Kanemitsu, Dynamics of Charged Excitons and Biexcitons in $CsPbBr_3$ Perovskite Nanocrystals Revealed by Femtosecond Transient-Absorption and Single-Dot Luminescence Spectroscopy, *J. Phys. Chem. Lett.*, 2017, **8**, 1413–1418.

29 H. Utzat, W. Sun, A. E. K. Kaplan, F. Krieg, M. Ginterseder, B. Spokoyny, N. D. Klein, K. E. Shulenberger, C. F. Perkinson, M. V Kovalenko and M. G. Bawendi, Coherent single-photon emission from colloidal lead halide perovskite quantum dots, *Science*, 2019, **363**, 1068–1072.

30 A. Pisoni, J. Jaćimović, O. S. Barišić, M. Spina, R. Gaál, L. Forró and E. Horváth, Ultra-low thermal conductivity in organic-inorganic hybrid perovskite $CH_3NH_3PbI_3$, *J. Phys. Chem. Lett.*, 2014, **5**, 2488–2492.

31 Y. Kawamura, H. Mashiyama and K. Hasebe, Structural Study on Cubic–Tetragonal Transition of $CH_3NH_3PbI_3$, *J. Phys. Soc. Japan*, 2002, **71**, 1694–1697.

32 Y. Yamada, T. Nakamura, M. Endo, A. Wakamiya and Y. Kanemitsu, Near-band-edge optical responses of solution-processed organic–inorganic hybrid perovskite $CH_3NH_3PbI_3$ on mesoporous TiO_2 electrodes, *Appl. Phys. Express*, 2014, **7**, 032302.

33 A. M. A. Leguy, P. Azarhoosh, M. I. Alonso, M. Campoy-Quiles, O. J. Weber, J. Yao, D. Bryant, M. T. Weller, J. Nelson, A. Walsh, M. van Schilfgaarde and P. R. F. Barnes, Experimental and theoretical optical properties of methylammonium lead halide perovskites, *Nanoscale*, 2016, **8**, 6317–6327.

34 Y. Yamada, T. Nakamura, M. Endo, A. Wakamiya and Y. Kanemitsu, Photocarrier recombination dynamics in perovskite $CH_3NH_3PbI_3$ for solar cell applications, *J. Am. Chem. Soc.*, 2014, **136**, 11610–11613.

35 S. D. Stranks, V. M. Burlakov, T. Leijtens, J. M. Ball, A. Goriely and H. J. Snaith, Recombination Kinetics in Organic-Inorganic Perovskites: Excitons, Free Charge, and Subgap States, *Phys. Rev. Appl.*, 2014, **2**, 034007.

36 F. Deschler, M. Price, S. Pathak, L. E. Klintberg, D. D. Jarausch, R. Higler, S. Hüttner, T. Leijtens, S. D.

Stranks, H. J. Snaith, M. Atatüre, R. T. Phillips and R. H. Friend, High photoluminescence efficiency and optically pumped lasing in solution-processed mixed halide perovskite semiconductors, *J. Phys. Chem. Lett.*, 2014, **5**, 1421–1426.

37 T. Yamada, Y. Yamada, H. Nishimura, Y. Nakaike, A. Wakamiya, Y. Murata and Y. Kanemitsu, Fast Free-Carrier Diffusion in $CH_3NH_3PbBr_3$ Single Crystals Revealed by Time-Resolved One- and Two-Photon Excitation Photoluminescence Spectroscopy, *Adv. Electron. Mater.*, 2016, **2**, 1500290.

38 T. Umebayashi, K. Asai, T. Kondo and A. Nakao, Electronic structures of lead iodide based low-dimensional crystals, *Phys. Rev. B*, 2003, **67**, 155405.

39 G. Giorgi, J. I. Fujisawa, H. Segawa and K. Yamashita, Small photocarrier effective masses featuring ambipolar transport in methylammonium lead iodide perovskite: A density functional analysis, *J. Phys. Chem. Lett.*, 2013, **4**, 4213–4216.

40 P. Umari, E. Mosconi and F. De Angelis, Relativistic GW calculations on $CH_3NH_3PbI_3$ and $CH_3NH_3SnI_3$ Perovskites for Solar Cell Applications, *Sci. Rep.*, 2015, **4**, 4467.

41 J. Even, L. Pedesseau, C. Katan, M. Kepenekian, J.-S. S. Lauret, D. Sapori and E. Deleporte, Solid-state physics perspective on hybrid perovskite semiconductors, *J. Phys. Chem. C*, 2015, **119**, 10161–10177.

42 W.-J. Yin, T. Shi and Y. Yan, Unusual defect physics in $CH_3NH_3PbI_3$ perovskite solar cell absorber, *Appl. Phys. Lett.*, 2014, **104**, 063903.

43 R. E. Brandt, V. Stevanović, D. S. Ginley and T. Buonassisi, Identifying defect-tolerant semiconductors with high minority-carrier lifetimes: Beyond hybrid lead halide perovskites, *MRS Commun.*, 2015, **5**, 265–275.

44 J. Even, L. Pedesseau, J. M. Jancu and C. Katan, Importance of spin-orbit coupling in hybrid organic/inorganic perovskites for photovoltaic applications, *J. Phys. Chem. Lett.*, 2013, **4**, 2999–3005.

45 J. H. Noh, S. H. Im, J. H. Heo, T. N. Mandal and S. Il Seok, Chemical Management for Colorful, Efficient, and Stable Inorganic–Organic Hybrid Nanostructured Solar Cells, *Nano Lett.*, 2013, **13**, 1764–1769.

46 G. E. Eperon, S. D. Stranks, C. Menelaou, M. B. Johnston, L. M. Herz and H. J. Snaith, Formamidinium lead trihalide: a broadly tunable perovskite for efficient planar heterojunction solar cells, *Energy Environ. Sci.*, 2014, **7**, 982.

47 F. Hao, C. C. Stoumpos, R. P. H. Chang and M. G. Kanatzidis, Anomalous band gap behavior in mixed Sn and Pb perovskites enables broadening of absorption spectrum in solar cells, *J. Am. Chem. Soc.*, 2014, **136**, 8094–8099.

48 E. T. Hoke, D. J. Slotcavage, E. R. Dohner, A. R. Bowring, H. I. Karunadasa and M. D. McGehee, Reversible photo-induced trap formation in mixed-halide hybrid perovskites for photovoltaics, *Chem. Sci.*, 2015, **6**, 613–617.

49 P. Löper, S.-J. Moon, S. Martín de Nicolas, B. Niesen, M. Ledinsky, S. Nicolay, J. Bailat, J.-H. Yum, S. De Wolf and C. Ballif, Organic–inorganic halide perovskite/crystalline silicon four-terminal tandem solar cells, *Phys. Chem. Chem. Phys.*, 2015, **17**, 1619–1629.

50 D. P. McMeekin, G. Sadoughi, W. Rehman, G. E. Eperon, M. Saliba, M. T. Horantner, A. Haghighirad, N. Sakai, L. Korte, B. Rech, M. B. Johnston, L. M. Herz and H. J. Snaith, A mixed-cation lead mixed-

halide perovskite absorber for tandem solar cells, *Science*, 2016, **351**, 151–155.

51 G. E. Eperon, T. Leijtens, K. A. Bush, R. Prasanna, T. Green, J. T.-W. Wang, D. P. McMeekin, G. Volonakis, R. L. Milot, R. May, A. Palmstrom, D. J. Slotcavage, R. A. Belisle, J. B. Patel, E. S. Parrott, R. J. Sutton, W. Ma, F. Moghadam, B. Conings, A. Babayigit, H. Boyen, S. Bent, F. Giustino, L. M. Herz, M. B. Johnston, M. D. McGehee and H. J. Snaith, Perovskite-perovskite tandem photovoltaics with optimized band gaps, *Science*, 2016, **354**, 861–865.

52 F. Sahli, J. Werner, B. A. Kamino, M. Bräuninger, R. Monnard, B. Paviet-Salomon, L. Barraud, L. Ding, J. J. Diaz Leon, D. Sacchetto, G. Cattaneo, M. Despeisse, M. Boccard, S. Nicolay, Q. Jeangros, B. Niesen and C. Ballif, Fully textured monolithic perovskite/silicon tandem solar cells with 25.2% power conversion efficiency, *Nat. Mater.*, 2018, **17**, 820–826.

53 J. Tong, Z. Song, D. H. Kim, X. Chen, C. Chen, A. F. Palmstrom, P. F. Ndione, M. O. Reese, S. P. Dunfield, O. G. Reid, J. Liu, F. Zhang, S. P. Harvey, Z. Li, S. T. Christensen, G. Teeter, D. Zhao, M. M. Al-Jassim, M. F. A. M. van Hest, M. C. Beard, S. E. Shaheen, J. J. Berry, Y. Yan and K. Zhu, Carrier lifetimes of >1 μs in Sn-Pb perovskites enable efficient all-perovskite tandem solar cells, *Science*, 2019, **364**, 475–479.

54 Y. Hou, E. Aydin, M. De Bastiani, C. Xiao, F. H. Isikgor, D.-J. Xue, B. Chen, H. Chen, B. Bahrami, A. H. Chowdhury, A. Johnston, S.-W. Baek, Z. Huang, M. Wei, Y. Dong, J. Troughton, R. Jalmood, A. J. Mirabelli, T. G. Allen, E. Van Kerschaver, M. I. Saidaminov, D. Baran, Q. Qiao, K. Zhu, S. De Wolf and E. H. Sargent, Efficient tandem solar cells with solution-processed perovskite on textured crystalline silicon, *Science*, 2020, **367**, 1135–1140.

55 J. Xu, C. C. Boyd, Z. J. Yu, A. F. Palmstrom, D. J. Witter, B. W. Larson, R. M. France, J. Werner, S. P. Harvey, E. J. Wolf, W. Weigand, S. Manzoor, M. F. A. M. van Hest, J. J. Berry, J. M. Luther, Z. C. Holman and M. D. McGehee, Triple-halide wide–band gap perovskites with suppressed phase segregation for efficient tandems, *Science*, 2020, **367**, 1097–1104.

56 D. Kim, H. J. Jung, I. J. Park, B. W. Larson, S. P. Dunfield, C. Xiao, J. Kim, J. Tong, P. Boonmongkolras, S. G. Ji, F. Zhang, S. R. Pae, M. Kim, S. B. Kang, V. Dravid, J. J. Berry, J. Y. Kim, K. Zhu, D. H. Kim and B. Shin, Efficient, stable silicon tandem cells enabled by anion-engineered wide-bandgap perovskites, *Science*, 2020, **368**, 155–160.

57 Z. Li, M. Yang, J. S. Park, S. H. Wei, J. J. Berry and K. Zhu, Stabilizing Perovskite Structures by Tuning Tolerance Factor: Formation of Formamidinium and Cesium Lead Iodide Solid-State Alloys, *Chem. Mater.*, 2016, **28**, 284–292.

58 M. Saliba, T. Matsui, J.-Y. Seo, K. Domanski, J.-P. Correa-Baena, M. K. Nazeeruddin, S. M. Zakeeruddin, W. Tress, A. Abate, A. Hagfeldt and M. Grätzel, Cesium-containing triple cation perovskite solar cells: improved stability, reproducibility and high efficiency, *Energy Environ. Sci.*, 2016, **9**, 1989–1997.

59 J.-P. Correa-Baena, M. Saliba, T. Buonassisi, M. Grätzel, A. Abate, W. Tress and A. Hagfeldt, Promises and challenges of perovskite solar cells, *Science*, 2017, **358**, 739–744.

60 S. Tao, I. Schmidt, G. Brocks, J. Jiang, I. Tranca, K. Meerholz and S. Olthof, Absolute energy level positions in tin- and lead-based halide perovskites, *Nat. Commun.*, 2019, **10**, 2560.

61 T. Yokoyama, D. H. Cao, C. C. Stoumpos, T.-B. Song, Y. Sato, S. Aramaki and M. G. Kanatzidis,

Overcoming Short-Circuit in Lead-Free $CH_3NH_3SnI_3$ Perovskite Solar Cells via Kinetically Controlled Gas–Solid Reaction Film Fabrication Process, *J. Phys. Chem. Lett.*, 2016, **7**, 776–782.

62 T. Handa, T. Yamada, H. Kubota, S. Ise, Y. Miyamoto and Y. Kanemitsu, Photocarrier Recombination and Injection Dynamics in Long-Term Stable Lead-Free $CH_3NH_3SnI_3$ Perovskite Thin Films and Solar Cells, *J. Phys. Chem. C*, 2017, **121**, 16158–16165.

63 M. Ozaki, Y. Katsuki, J. Liu, T. Handa, R. Nishikubo, S. Yakumaru, Y. Hashikawa, Y. Murata, T. Saito, Y. Shimakawa, Y. Kanemitsu, A. Saeki and A. Wakamiya, Solvent-Coordinated Tin Halide Complexes as Purified Precursors for Tin-Based Perovskites, *ACS Omega*, 2017, **2**, 7016–7021.

64 R. Nishikubo, N. Ishida, Y. Katsuki, A. Wakamiya and A. Saeki, Minute-Scale Degradation and Shift of Valence-Band Maxima of $(CH_3NH_3)PbI_3$ and $HC(NH_2)_2SnI_3$ Perovskites upon Air Exposure, *J. Phys. Chem. C*, 2017, **121**, 19650–19656.

65 R. Comin, G. Walters, E. S. Thibau, O. Voznyy, Z. H. Lu and E. H. Sargent, Structural, optical, and electronic studies of wide-bandgap lead halide perovskites, *J. Mater. Chem. C*, 2015, **3**, 8839–8843.

66 P. Fedeli, F. Gazza, D. Calestani, P. Ferro, T. Besagni, A. Zappettini, G. Calestani, E. Marchi, P. Ceroni and R. Mosca, Influence of the Synthetic Procedures on the Structural and Optical Properties of Mixed-Halide (Br, I) Perovskite Films, *J. Phys. Chem. C*, 2015, **119**, 21304–21313.

67 R. Prasanna, A. Gold-Parker, T. Leijtens, B. Conings, A. Babayigit, H. G. Boyen, M. F. Toney and M. D. McGehee, Band Gap Tuning via Lattice Contraction and Octahedral Tilting in Perovskite Materials for Photovoltaics, *J. Am. Chem. Soc.*, 2017, **139**, 11117–11124.

68 K. Galkowski, A. Mitioglu, A. Miyata, P. Plochocka, O. Portugall, G. E. Eperon, J. T.-W. Wang, T. Stergiopoulos, S. D. Stranks, H. J. Snaith and R. J. Nicholas, Determination of the exciton binding energy and effective masses for methylammonium and formamidinium lead tri-halide perovskite semiconductors, *Energy Environ. Sci.*, 2016, **9**, 962–970.

69 Y. Yamada, T. Yamada and Y. Kanemitsu, Free Carrier Radiative Recombination and Photon Recycling in Lead Halide Perovskite Solar Cell Materials, *Bull. Chem. Soc. Jpn.*, 2017, **90**, 1129–1140.

70 Y. Yamada, H. Mino, T. Kawahara, K. Oto, H. Suzuura and Y. Kanemitsu, Polaron Mass and Exciton Energy of $CH_3NH_3PbX_3$ Revealed by Landau Level Spectroscopy Under Low Magnetic Fields, *arXiv*, 2020, 2001.07901v2.

71 Y. Yamada, T. Nakamura, M. Endo, A. Wakamiya and Y. Kanemitsu, Photoelectronic Responses in Solution-Processed Perovskite $CH_3NH_3PbI_3$ Solar Cells Studied by Photoluminescence and Photoabsorption Spectroscopy, *IEEE J. Photovoltaics*, 2015, **5**, 401–405.

72 A. Miyata, A. Mitioglu, P. Plochocka, O. Portugall, J. T.-W. Wang, S. D. Stranks, H. J. Snaith and R. J. Nicholas, Direct measurement of the exciton binding energy and effective masses for charge carriers in organic–inorganic tri-halide perovskites, *Nat. Phys.*, 2015, **11**, 582–587.

73 T. Yamada, T. Aharen and Y. Kanemitsu, Near-Band-Edge Optical Responses of $CH_3NH_3PbCl_3$ Single Crystals: Photon Recycling of Excitonic Luminescence, *Phys. Rev. Lett.*, 2018, **120**, 057404.

74 J. Liu, M. Ozaki, S. Yakumaru, T. Handa, R. Nishikubo, Y. Kanemitsu, A. Saeki, Y. Murata, R. Murdey and A. Wakamiya, Lead-Free Solar Cells based on Tin Halide Perovskite Films with High Coverage and

Improved Aggregation, *Angew. Chemie Int. Ed.*, 2018, **57**, 13221–13225.

75 W. Ke and M. G. Kanatzidis, Prospects for low-toxicity lead-free perovskite solar cells, *Nat. Commun.*, 2019, **10**, 965.

76 X. Jiang, F. Wang, Q. Wei, H. Li, Y. Shang, W. Zhou, C. Wang, P. Cheng, Q. Chen, L. Chen and Z. Ning, Ultra-high open-circuit voltage of tin perovskite solar cells via an electron transporting layer design, *Nat. Commun.*, 2020, **11**, 1245.

77 X. Liu, Y. Wang, T. Wu, X. He, X. Meng, J. Barbaud, H. Chen, H. Segawa, X. Yang and L. Han, Efficient and stable tin perovskite solar cells enabled by amorphous-polycrystalline structure, *Nat. Commun.*, 2020, **11**, 2678.

78 T. Nakamura, S. Yakumaru, M. A. Truong, K. Kim, J. Liu, S. Hu, K. Otsuka, R. Hashimoto, R. Murdey, T. Sasamori, H. Do Kim, H. Ohkita, T. Handa, Y. Kanemitsu and A. Wakamiya, Sn(IV)-free tin perovskite films realized by in situ Sn(0) nanoparticle treatment of the precursor solution, *Nat. Commun.*, 2020, **11**, 3008.

79 T. Handa, A. Wakamiya and Y. Kanemitsu, Photophysics of lead-free tin halide perovskite films and solar cells, *APL Mater.*, 2019, **7**, 080903.

80 P. Y. Yu and M. Cardona, *Fundamentals of Semiconductors*, Springer, Berlin, 4th ed., 2010.

81 F. Brivio, J. M. Frost, J. M. Skelton, A. J. Jackson, O. J. Weber, M. T. Weller, A. R. Goñi, A. M. A. Leguy, P. R. F. Barnes and A. Walsh, Lattice dynamics and vibrational spectra of the orthorhombic, tetragonal, and cubic phases of methylammonium lead iodide, *Phys. Rev. B*, 2015, **92**, 144308.

82 A. Mattoni, A. Filippetti, M. I. Saba, C. Caddeo and P. Delugas, Temperature Evolution of Methylammonium Trihalide Vibrations at the Atomic Scale, *J. Phys. Chem. Lett.*, 2016, **7**, 529–535.

83 H. Zhu, K. Miyata, Y. Fu, J. Wang, P. P. Joshi, D. Niesner, K. W. Williams, S. Jin and X.-Y. Zhu, Screening in crystalline liquids protects energetic carriers in hybrid perovskites, *Science*, 2016, **353**, 1409–1413.

84 O. Yaffe, Y. Guo, L. Z. Tan, D. A. Egger, T. Hull, C. C. Stoumpos, F. Zheng, T. F. Heinz, L. Kronik, M. G. Kanatzidis, J. S. Owen, A. M. Rappe, M. A. Pimenta and L. E. Brus, Local Polar Fluctuations in Lead Halide Perovskite Crystals, *Phys. Rev. Lett.*, 2017, **118**, 136001.

85 M. Nagai, T. Tomioka, M. Ashida, M. Hoyano, R. Akashi, Y. Yamada, T. Aharen and Y. Kanemitsu, Longitudinal Optical Phonons Modified by Organic Molecular Cation Motions in Organic-Inorganic Hybrid Perovskites, *Phys. Rev. Lett.*, 2018, **121**, 145506.

86 A. M. A. Leguy, A. R. Goñi, J. M. Frost, J. Skelton, F. Brivio, X. Rodríguez-Martínez, O. J. Weber, A. Pallipurath, M. I. Alonso, M. Campoy-Quiles, M. T. Weller, J. Nelson, A. Walsh and P. R. F. Barnes, Dynamic disorder, phonon lifetimes, and the assignment of modes to the vibrational spectra of methylammonium lead halide perovskites, *Phys. Chem. Chem. Phys.*, 2016, **18**, 27051–27066.

87 C. Quarti, G. Grancini, E. Mosconi, P. Bruno, J. M. Ball, M. M. Lee, H. J. Snaith, A. Petrozza and F. De Angelis, The Raman spectrum of the $CH_3NH_3PbI_3$ hybrid perovskite: Interplay of theory and experiment, *J. Phys. Chem. Lett.*, 2014, **5**, 279–284.

88 C. La-o-vorakiat, H. Xia, J. Kadro, T. Salim, D. Zhao, T. Ahmed, Y. M. Lam, J.-X. Zhu, R. A. Marcus,

M.-E. Michel-Beyerle and E. E. M. Chia, Phonon Mode Transformation Across the Orthohombic–Tetragonal Phase Transition in a Lead Iodide Perovskite $CH_3NH_3PbI_3$: A Terahertz Time-Domain Spectroscopy Approach, *J. Phys. Chem. Lett.*, 2016, **7**, 1–6.

89 R. G. Niemann, A. G. Kontos, D. Palles, E. I. Kamitsos, A. Kaltzoglou, F. Brivio, P. Falaras and P. J. Cameron, Halogen Effects on Ordering and Bonding of $CH_3NH_3^+$ in $CH_3NH_3PbX_3$ (X = Cl, Br, I) Hybrid Perovskites: A Vibrational Spectroscopic Study, *J. Phys. Chem. C*, 2016, **120**, 2509–2519.

90 M. Sendner, P. K. Nayak, D. A. Egger, S. Beck, C. Müller, B. Epding, W. Kowalsky, L. Kronik, H. J. Snaith, A. Pucci and R. Lovrinčić, Optical phonons in methylammonium lead halide perovskites and implications for charge transport, *Mater. Horizons*, 2016, **3**, 613–620.

91 D. Zhao, J. M. Skelton, H. Hu, C. La-o-vorakiat, J.-X. Zhu, R. A. Marcus, M.-E. Michel-Beyerle, Y. M. Lam, A. Walsh and E. E. M. Chia, Low-frequency optical phonon modes and carrier mobility in the halide perovskite $CH_3NH_3PbBr_3$ using terahertz time-domain spectroscopy, *Appl. Phys. Lett.*, 2017, **111**, 201903.

92 A. D. Wright, C. Verdi, R. L. Milot, G. E. Eperon, M. A. Pérez-Osorio, H. J. Snaith, F. Giustino, M. B. Johnston and L. M. Herz, Electron-phonon coupling in hybrid lead halide perovskites, *Nat. Commun.*, 2016, **7**, 11755.

93 L. Q. Phuong, Y. Nakaike, A. Wakamiya and Y. Kanemitsu, Free Excitons and Exciton–Phonon Coupling in $CH_3NH_3PbI_3$ Single Crystals Revealed by Photocurrent and Photoluminescence Measurements at Low Temperatures, *J. Phys. Chem. Lett.*, 2016, **7**, 4905–4910.

94 F. Gervais and B. Piriou, Temperature dependence of transverse- and longitudinal-optic modes in TiO_2 (rutile), *Phys. Rev. B*, 1974, **10**, 1642–1654.

95 T. Kirchartz, T. Markvart, U. Rau and D. A. Egger, Impact of Small Phonon Energies on the Charge-Carrier Lifetimes in Metal-Halide Perovskites, *J. Phys. Chem. Lett.*, 2018, **9**, 939–946.

96 Y. Kanemitsu, T. Yamada, T. Handa and M. Nagai, Optical responses of lead halide perovskite semiconductors, *Semicond. Sci. Technol.*, 2020, **35**, 093001.

97 P. G. Klemens, Anharmonic decay of optical phonon in diamond, *Phys. Rev. B*, 1975, **11**, 3206–3207.

98 T. Yamada, T. Aharen and Y. Kanemitsu, Up-converted photoluminescence from $CH_3NH_3PbI_3$ perovskite semiconductors: Implications for laser cooling, *Phys. Rev. Mater.*, 2019, **3**, 024601.

99 C. Wehrenfennig, M. Liu, H. J. Snaith, M. B. Johnston and L. M. Herz, Homogeneous Emission Line Broadening in the Organo Lead Halide Perovskite $CH_3NH_3PbI_{3-x}Cl_x$, *J. Phys. Chem. Lett.*, 2014, **5**, 1300–1306.

100 T. Handa, T. Aharen, A. Wakamiya and Y. Kanemitsu, Radiative recombination and electron-phonon coupling in lead-free $CH_3NH_3SnI_3$ perovskite thin film, *Phys. Rev. Mater.*, 2018, **2**, 075402.

101 O. Pfingsten, J. Klein, L. Protesescu, M. I. Bodnarchuk, M. V. Kovalenko and G. Bacher, Phonon Interaction and Phase Transition in Single Formamidinium Lead Bromide Quantum Dots, *Nano Lett.*, 2018, **18**, 4440–4446.

102 M. Fu, P. Tamarat, J.-B. Trebbia, M. I. Bodnarchuk, M. V. Kovalenko, J. Even and B. Lounis, Unraveling exciton–phonon coupling in individual $FAPbI_3$ nanocrystals emitting near-infrared single photons, *Nat. Commun.*, 2018, **9**, 3318.

103 J. Ramade, L. M. Andriambariarijaona, V. Steinmetz, N. Goubet, L. Legrand, T. Barisien, F. Bernardot, C. Testelin, E. Lhuillier, A. Bramati and M. Chamarro, Exciton-phonon coupling in a $CsPbBr_3$ single nanocrystal, *Appl. Phys. Lett.*, 2018, **112**, 072104.

104 S. Masada, T. Yamada, H. Tahara, H. Hirori, M. Saruyama, T. Kawawaki, R. Sato, T. Teranishi and Y. Kanemitsu, Effect of A-Site Cation on Photoluminescence Spectra of Single Lead Bromide Perovskite Nanocrystals, *Nano Lett.*, 2020, **20**, 4022–4028.

105 S.-T. Ha, C. Shen, J. Zhang and Q. Xiong, Laser cooling of organic–inorganic lead halide perovskites, *Nat. Photonics*, 2016, **10**, 115–121.

106 T. Yamada, T. Aharen and Y. Kanemitsu, Upconverted excitonic photoluminescence from a two-dimensional lead-halide perovskite, *J. Chem. Phys.*, 2019, **151**, 234709.

107 W. van Roosbroeck and W. Shockley, Photon-radiative recombination of electrons and holes in germanium, *Phys. Rev.*, 1954, **94**, 1558–1560.

108 E. Daub and P. Wurfel, Ultralow values of the absorption coefficient of Si obtained from luminescence, *Phys. Rev. Lett.*, 1995, **74**, 1020–1023.

109 C. Barugkin, J. Cong, T. Duong, S. Rahman, H. T. Nguyen, D. Macdonald, T. P. White and K. R. Catchpole, Ultralow Absorption Coefficient and Temperature Dependence of Radiative Recombination of $CH_3NH_3PbI_3$ Perovskite from Photoluminescence, *J. Phys. Chem. Lett.*, 2015, **6**, 767–772.

110 F. Staub, H. Hempel, J. C. Hebig, J. Mock, U. W. Paetzold, U. Rau, T. Unold and T. Kirchartz, Beyond Bulk Lifetimes: Insights into Lead Halide Perovskite Films from Time-Resolved Photoluminescence, *Phys. Rev. Appl.*, 2016, **6**, 044017.

111 Y. Yamada, T. Yamada, L. Q. Phuong, N. Maruyama, H. Nishimura, A. Wakamiya, Y. Murata and Y. Kanemitsu, Dynamic Optical Properties of $CH_3NH_3PbI_3$ Single Crystals As Revealed by One- and Two-Photon Excited Photoluminescence Measurements, *J. Am. Chem. Soc.*, 2015, **137**, 10456–10459.

112 T. Yamada, Y. Yamada, Y. Nakaike, A. Wakamiya and Y. Kanemitsu, Photon Emission and Reabsorption Processes in $CH_3NH_3PbBr_3$ Single Crystals Revealed by Time-Resolved Two-Photon-Excitation Photoluminescence Microscopy, *Phys. Rev. Appl.*, 2017, **7**, 014001.

113 O. D. Miller, E. Yablonovitch and S. R. Kurtz, Strong Internal and External Luminescence as Solar Cells Approach the Shockley–Queisser Limit, *IEEE J. Photovoltaics*, 2012, **2**, 303–311.

114 L. M. Pazos-Outon, M. Szumilo, R. Lamboll, J. M. Richter, M. Crespo-Quesada, M. Abdi-Jalebi, H. J. Beeson, M. Vru ini, M. Alsari, H. J. Snaith, B. Ehrler, R. H. Friend and F. Deschler, Photon recycling in lead iodide perovskite solar cells, *Science*, 2016, **351**, 1430–1433.

115 J. M. Richter, M. Abdi-Jalebi, A. Sadhanala, M. Tabachnyk, J. P. H. Rivett, L. M. Pazos-Outón, K. C. Gödel, M. Price, F. Deschler and R. H. Friend, Enhancing photoluminescence yields in lead halide perovskites by photon recycling and light out-coupling, *Nat. Commun.*, 2016, **7**, 13941.

116 Y. Fang, H. Wei, Q. Dong and J. Huang, Quantification of re-absorption and re-emission processes to determine photon recycling efficiency in perovskite single crystals, *Nat. Commun.*, 2017, **8**, 14417.

117 Y. Yamada, M. Hoyano, R. Akashi, K. Oto and Y. Kanemitsu, Impact of Chemical Doping on Optical Responses in Bismuth-Doped $CH_3NH_3PbBr_3$ Single Crystals: Carrier Lifetime and Photon Recycling, *J.*

Phys. Chem. Lett., 2017, **8**, 5798–5803.

118 L. M. Pazos-Outón, T. P. Xiao and E. Yablonovitch, Fundamental Efficiency Limit of Lead Iodide Perovskite Solar Cells, *J. Phys. Chem. Lett.*, 2018, **9**, 1703–1711.

119 K. Kojima, K. Ikemura, K. Matsumori, Y. Yamada, Y. Kanemitsu and S. F. Chichibu, Internal quantum efficiency of radiation in a bulk $CH_3NH_3PbBr_3$ perovskite crystal quantified by using the omnidirectional photoluminescence spectroscopy, *APL Mater.*, 2019, **7**, 071116.

120 T. Tiedje, Band tail recombination limit to the output voltage of amorphous silicon solar cells, *Appl. Phys. Lett.*, 1982, **40**, 627–629.

121 U. Rau and J. H. Werner, Radiative efficiency limits of solar cells with lateral band-gap fluctuations, *Appl. Phys. Lett.*, 2004, **84**, 3735–3737.

122 C.-H. H. M. Chuang, A. Maurano, R. E. Brandt, G. W. Hwang, J. Jean, T. Buonassisi, V. Bulović and M. G. Bawendi, Open-Circuit Voltage Deficit, Radiative Sub-Bandgap States, and Prospects in Quantum Dot Solar Cells, *Nano Lett.*, 2015, **15**, 3286–3294.

123 L. Zhu, H. Akiyama and Y. Kanemitsu, Intrinsic and extrinsic drops in open-circuit voltage and conversion efficiency in solar cells with quantum dots embedded in host materials, *Sci. Rep.*, 2018, **8**, 11704.

124 Y. Toyozawa, *Optical Processes in Solids*, Cambridge University Press, Cambridge, 2003.

125 S. De Wolf, J. Holovsky, S.-J. Moon, P. Löper, B. Niesen, M. Ledinsky, F.-J. Haug, J.-H. Yum and C. Ballif, Organometallic Halide Perovskites: Sharp Optical Absorption Edge and Its Relation to Photovoltaic Performance, *J. Phys. Chem. Lett.*, 2014, **5**, 1035–1039.

126 M. Shirayama, H. Kadowaki, T. Miyadera, T. Sugita, M. Tamakoshi, M. Kato, T. Fujiseki, D. Murata, S. Hara, T. N. Murakami, S. Fujimoto, M. Chikamatsu and H. Fujiwara, Optical Transitions in Hybrid Perovskite Solar Cells: Ellipsometry, Density Functional Theory, and Quantum Efficiency Analyses for $CH_3NH_3PbI_3$, *Phys. Rev. Appl.*, 2016, **5**, 014012.

127 V. M. Kiyek, Y. A. Birkhölzer, Y. Smirnov, M. Ledinsky, Z. Remes, J. Momand, B. J. Kooi, G. Koster, G. Rijnders and M. Morales-Masis, Single-Source, Solvent-Free, Room Temperature Deposition of Black γ-$CsSnI_3$ Films, *Adv. Mater. Interfaces*, 2020, **7**, 2000162.

128 Y. Yang, D. P. Ostrowski, R. M. France, K. Zhu, J. van de Lagemaat, J. M. Luther and M. C. Beard, Observation of a hot-phonon bottleneck in lead-iodide perovskites, *Nat. Photonics*, 2016, **10**, 53–59.

129 M. B. Price, J. Butkus, T. C. Jellicoe, A. Sadhanala, A. Briane, J. E. Halpert, K. Broch, J. M. Hodgkiss, R. H. Friend and F. Deschler, Hot-carrier cooling and photoinduced refractive index changes in organic–inorganic lead halide perovskites, *Nat. Commun.*, 2015, **6**, 8420.

130 M. Li, S. Bhaumik, T. W. Goh, M. S. Kumar, N. Yantara, M. Grätzel, S. Mhaisalkar, N. Mathews and T. C. Sum, Slow cooling and highly efficient extraction of hot carriers in colloidal perovskite nanocrystals, *Nat. Commun.*, 2017, **8**, 14350.

131 M. Li, J. Fu, Q. Xu and T. C. Sum, Slow Hot-Carrier Cooling in Halide Perovskites: Prospects for Hot-Carrier Solar Cells, *Adv. Mater.*, 2019, **31**, 1802486.

132 P. P. Joshi, S. F. Maehrlein and X. Zhu, Dynamic Screening and Slow Cooling of Hot Carriers in Lead Halide Perovskites, *Adv. Mater.*, 2019, **31**, 1803054.

133 S. Kahmann and M. A. Loi, Hot carrier solar cells and the potential of perovskites for breaking the Shockley–Queisser limit, *J. Mater. Chem. C*, 2019, **7**, 2471–2486.

134 W. Shockley and H. J. Queisser, Detailed Balance Limit of Efficiency of p-n Junction Solar Cells, *J. Appl. Phys.*, 1961, **32**, 510–519.

135 R. T. Ross and A. J. Nozik, Efficiency of hot-carrier solar energy converters, *J. Appl. Phys.*, 1982, **53**, 3813–3818.

136 P. Würfel, Solar energy conversion with hot electrons from impact ionisation, *Sol. Energy Mater. Sol. Cells*, 1997, **46**, 43–52.

137 D. König, K. Casalenuovo, Y. Takeda, G. Conibeer, J. F. Guillemoles, R. Patterson, L. M. Huang and M. A. Green, Hot carrier solar cells: Principles, materials and design, *Physica E*, 2010, **42**, 2862–2866.

138 S. Yakunin, L. Protesescu, F. Krieg, M. I. Bodnarchuk, G. Nedelcu, M. Humer, G. De Luca, M. Fiebig, W. Heiss and M. V. Kovalenko, Low-threshold amplified spontaneous emission and lasing from colloidal nanocrystals of caesium lead halide perovskites, *Nat. Commun.*, 2015, **6**, 8056.

139 G. Yumoto, H. Tahara, T. Kawawaki, M. Saruyama, R. Sato, T. Teranishi and Y. Kanemitsu, Hot Biexciton Effect on Optical Gain in $CsPbI_3$ Perovskite Nanocrystals, *J. Phys. Chem. Lett.*, 2018, **9**, 2222–2228.

140 G. Nagamine, J. O. Rocha, L. G. Bonato, A. F. Nogueira, Z. Zaharieva, A. A. R. Watt, C. H. de Brito Cruz and L. A. Padilha, Two-Photon Absorption and Two-Photon-Induced Gain in Perovskite Quantum Dots, *J. Phys. Chem. Lett.*, 2018, **9**, 3478–3484.

141 E. Kobiyama, H. Tahara, R. Sato, M. Saruyama, T. Teranishi and Y. Kanemitsu, Reduction of Optical Gain Threshold in $CsPbI_3$ Nanocrystals Achieved by Generation of Asymmetric Hot-Biexcitons, *Nano Lett.*, 2020, **20**, 3905–3910.

142 J. Fu, Q. Xu, G. Han, B. Wu, C. H. A. Huan, M. L. Leek and T. C. Sum, Hot carrier cooling mechanisms in halide perovskites, *Nat. Commun.*, 2017, **8**, 1300.

143 J. Yang, X. Wen, H. Xia, R. Sheng, Q. Ma, J. Kim, P. Tapping, T. Harada, T. W. Kee, F. Huang, Y.-B. Cheng, M. Green, A. Ho-Baillie, S. Huang, S. Shrestha, R. Patterson and G. Conibeer, Acoustic-optical phonon up-conversion and hot-phonon bottleneck in lead-halide perovskites, *Nat. Commun.*, 2017, **8**, 14120.

144 Q. Shen, T. S. Ripolles, J. Even, Y. Ogomi, K. Nishinaka, T. Izuishi, N. Nakazawa, Y. Zhang, C. Ding, F. Liu, T. Toyoda, K. Yoshino, T. Minemoto, K. Katayama and S. Hayase, Slow hot carrier cooling in cesium lead iodide perovskites, *Appl. Phys. Lett.*, 2017, **111**, 153903.

145 Y. Rosenwaks, M. C. Hanna, D. H. Levi, D. M. Szmyd, R. K. Ahrenkiel and A. J. Nozik, Hot-carrier cooling in GaAs: Quantum wells versus bulk, *Phys. Rev. B*, 1993, **48**, 14675–14678.

146 A. J. Nozik, Spectroscopy and hot electron relaxation dynamics in semiconductor quantum wells and quantum dots, *Annu. Rev. Phys. Chem.*, 2001, **52**, 193–231.

147 J. M. Frost, L. D. Whalley and A. Walsh, Slow Cooling of Hot Polarons in Halide Perovskite Solar Cells, *ACS Energy Lett.*, 2017, **2**, 2647–2652.

148 T. R. Hopper, A. Gorodetsky, J. M. Frost, C. Müller, R. Lovrincic and A. A. Bakulin, Ultrafast Intraband

Spectroscopy of Hot-Carrier Cooling in Lead-Halide Perovskites, *ACS Energy Lett.*, 2018, **3**, 2199–2205.

149 J. Chen, M. E. Messing, K. Zheng and T. Pullerits, Cation-Dependent Hot Carrier Cooling in Halide Perovskite Nanocrystals, *J. Am. Chem. Soc.*, 2019, **141**, 3532–3540.

150 Y. Kanemitsu, Trion dynamics in lead halide perovskite nanocrystals, *J. Chem. Phys.*, 2019, **151**, 170902.

151 N. Yarita, T. Aharen, H. Tahara, M. Saruyama, T. Kawawaki, R. Sato, T. Teranishi and Y. Kanemitsu, Observation of positive and negative trions in organic-inorganic hybrid perovskite nanocrystals, *Phys. Rev. Mater.*, 2018, **2**, 116003.

152 D. Niesner, H. Zhu, K. Miyata, P. P. Joshi, T. J. S. Evans, B. J. Kudisch, M. T. Trinh, M. Marks and X. Y. Zhu, Persistent Energetic Electrons in Methylammonium Lead Iodide Perovskite Thin Films, *J. Am. Chem. Soc.*, 2016, **138**, 15717–15726.

153 X. Y. Zhu and V. Podzorov, Charge Carriers in Hybrid Organic-Inorganic Lead Halide Perovskites Might Be Protected as Large Polarons, *J. Phys. Chem. Lett.*, 2015, **6**, 4758–4761.

154 S. A. Bretschneider, F. Laquai and M. Bonn, Trap-Free Hot Carrier Relaxation in Lead–Halide Perovskite Films, *J. Phys. Chem. C*, 2017, **121**, 11201–11206.

155 Z. Guo, Y. Wan, M. Yang, J. Snaider, K. Zhu and L. Huang, Long-range hot-carrier transport in hybrid perovskites visualized by ultrafast microscopy, *Science*, 2017, **356**, 59–62.

156 H.-H. Fang, S. Adjokatse, S. Shao, J. Even and M. A. Loi, Long-lived hot-carrier light emission and large blue shift in formamidinium tin triiodide perovskites, *Nat. Commun.*, 2018, **9**, 243.

157 C. A. Nelson, N. R. Monahan and X.-Y. Zhu, Exceeding the Shockley–Queisser limit in solar energy conversion, *Energy Environ. Sci.*, 2013, **6**, 3508.

158 Y. Rakita, S. R. Cohen, N. K. Kedem, G. Hodes and D. Cahen, Mechanical properties of $APbX_3$ (A = Cs or CH_3NH_3; X = I or Br) perovskite single crystals, *MRS Commun.*, 2015, **5**, 623–629.

159 A. C. Ferreira, A. Létoublon, S. Paofai, S. Raymond, C. Ecolivet, B. Rufflé, S. Cordier, C. Katan, M. I. Saidaminov, A. A. Zhumekenov, O. M. Bakr, J. Even and P. Bourges, Elastic Softness of Hybrid Lead Halide Perovskites, *Phys. Rev. Lett.*, 2018, **121**, 085502.

160 M. A. Haque, S. Kee, D. R. Villalva, W. Ong and D. Baran, Halide Perovskites: Thermal Transport and Prospects for Thermoelectricity, *Adv. Sci.*, 2020, **7**, 1903389.

161 M. Wang and S. Lin, Anisotropic and Ultralow Phonon Thermal Transport in Organic-Inorganic Hybrid Perovskites: Atomistic Insights into Solar Cell Thermal Management and Thermoelectric Energy Conversion Efficiency, *Adv. Funct. Mater.*, 2016, **26**, 5297–5306.

162 T. Hata, G. Giorgi and K. Yamashita, The Effects of the Organic–Inorganic Interactions on the Thermal Transport Properties of $CH_3NH_3PbI_3$, *Nano Lett.*, 2016, **16**, 2749–2753.

163 W. Lee, H. Li, A. B. Wong, D. Zhang, M. Lai, Y. Yu, Q. Kong, E. Lin, J. J. Urban, J. C. Grossman and P. Yang, Ultralow thermal conductivity in all-inorganic halide perovskites, *Proc. Natl. Acad. Sci.*, 2017, **114**, 8693–8697.

164 A. Kovalsky, L. Wang, G. T. Marek, C. Burda and J. S. Dyck, Thermal Conductivity of $CH_3NH_3PbI_3$ and $CsPbI_3$: Measuring the Effect of the Methylammonium Ion on Phonon Scattering, *J. Phys. Chem. C*, 2017, **121**, 3228–3233.

165 G. A. Elbaz, W. L. Ong, E. A. Doud, P. Kim, D. W. Paley, X. Roy and J. A. Malen, Phonon Speed, Not Scattering, Differentiates Thermal Transport in Lead Halide Perovskites, *Nano Lett.*, 2017, **17**, 5734–5739.

166 A. Gold-Parker, P. M. Gehring, J. M. Skelton, I. C. Smith, D. Parshall, J. M. Frost, H. I. Karunadasa, A. Walsh and M. F. Toney, Acoustic phonon lifetimes limit thermal transport in methylammonium lead iodide, *Proc. Natl. Acad. Sci.*, 2018, **115**, 11905–11910.

167 J. R. Whinnery, Laser measurement of optical absorption in liquids, *Acc. Chem. Res.*, 1974, **7**, 225–231.

168 T. Handa, H. Tahara, T. Aharen and Y. Kanemitsu, Large negative thermo-optic coefficients of a lead halide perovskite, *Sci. Adv.*, 2019, **5**, eaax0786.

169 D. H. Fabini, C. C. Stoumpos, G. Laurita, A. Kaltzoglou, A. G. Kontos, P. Falaras, M. G. Kanatzidis and R. Seshadri, Reentrant Structural and Optical Properties and Large Positive Thermal Expansion in Perovskite Formamidinium Lead Iodide, *Angew. Chemie Int. Ed.*, 2016, **55**, 15392–15396.

170 C. Ge, M. Hu, P. Wu, Q. Tan, Z. Chen, Y. Wang, J. Shi and J. Feng, Ultralow Thermal Conductivity and Ultrahigh Thermal Expansion of Single-Crystal Organic–Inorganic Hybrid Perovskite $CH_3NH_3PbX_3$ (X = Cl, Br, I), *J. Phys. Chem. C*, 2018, **122**, 15973–15978.

171 D. M. Trots and S. V. Myagkota, High-temperature structural evolution of caesium and rubidium triiodoplumbates, *J. Phys. Chem. Solids*, 2008, **69**, 2520–2526.

172 M. Bass, E. W. Van Stryland, D. R. Williams and W. L. Wolfe, *Handbook of Optics Volume II*, McGraw-Hill, 1995.

173 D. R. Lide, *CRC Handbook of Chemistry and Physics*, CRC Press, Boca Raton, FL, 2005.

174 E. C. Schueller, G. Laurita, D. H. Fabini, C. C. Stoumpos, M. G. Kanatzidis and R. Seshadri, Crystal Structure Evolution and Notable Thermal Expansion in Hybrid Perovskites Formamidinium Tin Iodide and Formamidinium Lead Bromide, *Inorg. Chem.*, 2018, **57**, 695–701.

175 M. Keshavarz, M. Ottesen, S. Wiedmann, M. Wharmby, R. Küchler, H. Yuan, E. Debroye, J. A. Steele, J. Martens, N. E. Hussey, M. Bremholm, M. B. J. Roeffaers and J. Hofkens, Tracking Structural Phase Transitions in Lead-Halide Perovskites by Means of Thermal Expansion, *Adv. Mater.*, 2019, **31**, 1900521.

176 Y. He and G. Galli, Perovskites for Solar Thermoelectric Applications: A First Principle Study of $CH_3NH_3AI_3$ (A = Pb and Sn), *Chem. Mater.*, 2014, **26**, 5394–5400.

177 X. Mettan, R. Pisoni, P. Matus, A. Pisoni, J. Jaćimović, B. Náfrádi, M. Spina, D. Pavuna, L. Forró and E. Horváth, Tuning of the Thermoelectric Figure of Merit of $CH_3NH_3MI_3$ (M═Pb,Sn) Photovoltaic Perovskites, *J. Phys. Chem. C*, 2015, **119**, 11506–11510.

178 B. J. Foley, D. L. Marlowe, K. Sun, W. A. Saidi, L. Scudiero, M. C. Gupta and J. J. Choi, Temperature dependent energy levels of methylammonium lead iodide perovskite, *Appl. Phys. Lett.*, 2015, **106**, 243904.

179 J. Lin, M. Lai, L. Dou, C. S. Kley, H. Chen, F. Peng, J. Sun, D. Lu, S. A. Hawks, C. Xie, F. Cui, A. P. Alivisatos, D. T. Limmer and P. Yang, Thermochromic halide perovskite solar cells, *Nat. Mater.*, 2018, **17**, 261–267.

180 S. Yakunin, B. M. Benin, Y. Shynkarenko, O. Nazarenko, M. I. Bodnarchuk, D. N. Dirin, C. Hofer, S. Cattaneo and M. V. Kovalenko, High-resolution remote thermometry and thermography using luminescent low-dimensional tin-halide perovskites, *Nat. Mater.*, 2019, **18**, 846–852.

181 M. Han and A. Wang, Temperature compensation of optical microresonators using a surface layer with negative thermo-optic coefficient, *Opt. Lett.*, 2007, **32**, 1800.

182 G. Ghosh, *Handbook of Thermo-Optic Coefficients of Optical Materials With Applications*, Academic Press, 1997.

183 T. Handa, H. Tahara, T. Aharen, A. Shimazaki, A. Wakamiya and Y. Kanemitsu, Large thermal expansion leads to negative thermo-optic coefficient of halide perovskite $CH_3NH_3PbCl_3$, *Phys. Rev. Mater.*, 2020, **4**, 074604.

184 P. Y. Yu and M. Cardona, Temperature Coefficient of the Refractive Index of Diamond- and Zinc-Blende-Type Semiconductors, *Phys. Rev. B*, 1970, **2**, 3193–3197.

185 Y. Tsay, B. Bendow and S. S. Mitra, Theory of the Temperature Derivative of the Refractive Index in Transparent Crystals, *Phys. Rev. B*, 1973, **8**, 2688–2696.

186 T. Soma, J. Satoh and H. Matsuo, Thermal expansion coefficient of GaAs and InP, *Solid State Commun.*, 1982, **42**, 889–892.

187 Y. Okada and Y. Tokumaru, Precise determination of lattice parameter and thermal expansion coefficient of silicon between 300 and 1500 K, *J. Appl. Phys.*, 1984, **56**, 314–320.

188 K. Wu, A. Bera, C. Ma, Y. Du, Y. Yang, L. Li and T. Wu, Temperature-dependent excitonic photoluminescence of hybrid organometal halide perovskite films, *Phys. Chem. Chem. Phys.*, 2014, **16**, 22476–22481.

189 M. I. Dar, G. Jacopin, S. Meloni, A. Mattoni, N. Arora, A. Boziki, S. M. Zakeeruddin, U. Rothlisberger and M. Grätzel, Origin of unusual bandgap shift and dual emission in organic-inorganic lead halide perovskites, *Sci. Adv.*, 2016, **2**, e1601156.

190 J. Tilchin, D. N. Dirin, G. I. Maikov, A. Sashchiuk, M. V. Kovalenko and E. Lifshitz, Hydrogen-like Wannier-Mott Excitons in Single Crystal of Methylammonium Lead Bromide Perovskite, *ACS Nano*, 2016, **10**, 6363–6371.

Figure Captions

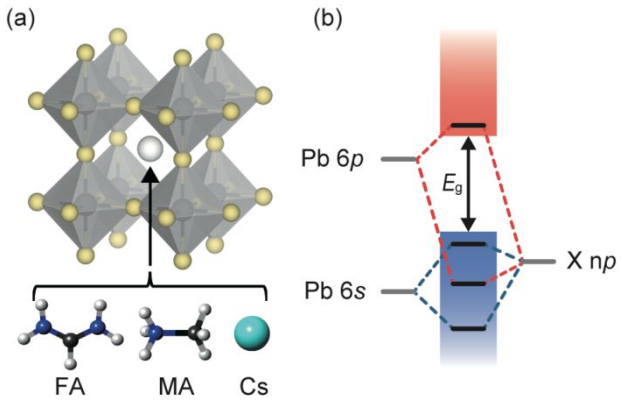

Fig. 1 (a) Illustration of the cubic lead halide perovskite crystal structure $APbX_3$. The halogen atoms are shown with the yellow spheres and are usually I, Br, or Cl. As the A-site cation located at the center of the PbX_6 octahedral network, the organic formamidinium (FA) and methylammonium (MA), or the inorganic Cs^+ can be incorporated. (b) Overview of the orbital characters of the electronic band structure in a lead halide perovskite. The state related to the A-site cation is located far below the band edge, and therefore it does not directly affect the bandgap energy (E_g).

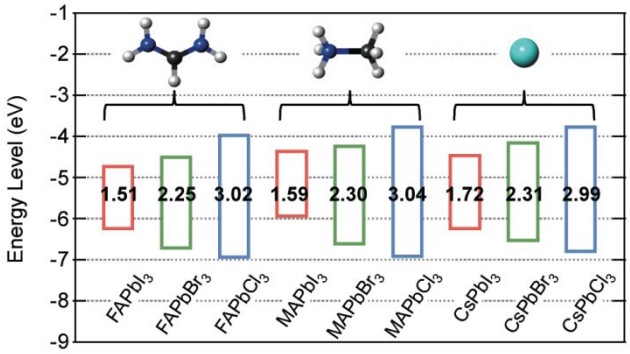

Fig. 2 Absolute energies of valence band maximum and conduction band minimum of nine representative lead halide perovskites. The values shown in the figure are the optical bandgap energies estimated from absorption measurements. The data used to prepare this graph are taken from ref. 60.

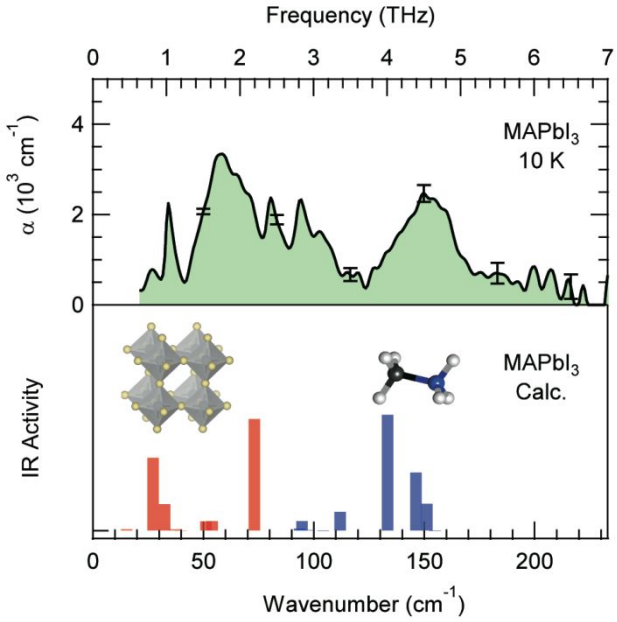

Fig. 3 Measured absorption coefficient (top panel) and calculated infrared activity (bottom panel) for the low-temperature orthorhombic phase of $MAPbI_3$ in the range 0–233 cm^{-1}, which includes phonon modes of the inorganic PbI_6 cage (red bars) and vibrations of the molecular cation (blue bars). The absorption coefficient $\alpha = (2\omega/c)\mathrm{Im}[\epsilon^{1/2}]$ is plotted from the complex values of ϵ in ref. 85. Error bars are added with the assumption of $|\Delta n| < 0.1$. The infrared activity is plotted using the calculated values and assignments in ref. 81 and 86.

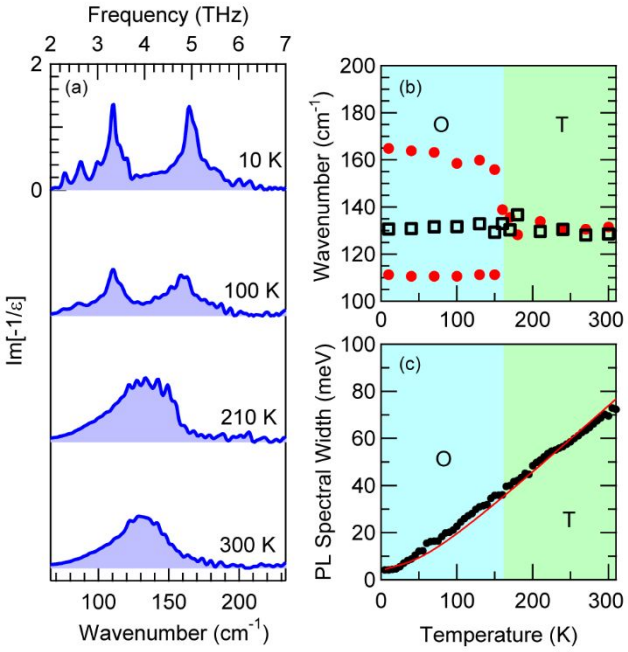

Fig. 4 (a) The energy loss function Im[-1/ϵ] of the $MAPbI_3$ single crystal at different temperatures. (b) Peak wavenumbers (closed red circles) and effective wavenumbers (open black squares) of the LO phonons as a function of temperature. (c) The temperature dependence of the spectral width of the luminescence from the free exciton. The red curve shows the predicted width including the effects of acoustic and LO phonon interactions. The labels O and T represent the orthorhombic and tetragonal phases, respectively. Adapted from ref. 85.

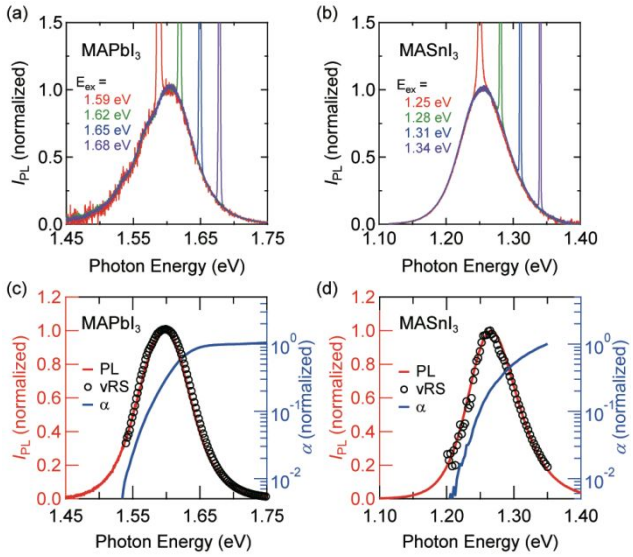

Fig. 5 Room-temperature PL spectra for resonant excitation of (a) $MAPbI_3$ and (b) $MASnI_3$ thin films. The spectral shapes are independent of the excitation energy, *i.e.* these data show homogeneous broadening. The sharp peaks in the figures represent the scattering of the excitation light. PL (red curve) and absorption (blue curve) spectra for (c) $MAPbI_3$ and (d) $MASnI_3$ thin films. The open circles represent the spontaneous emission spectra calculated from the absorption spectra using the van Roosbroeck–Shockley relation (vRS). Data in panels (a) and (b) are taken from ref. 98 and 62, respectively.

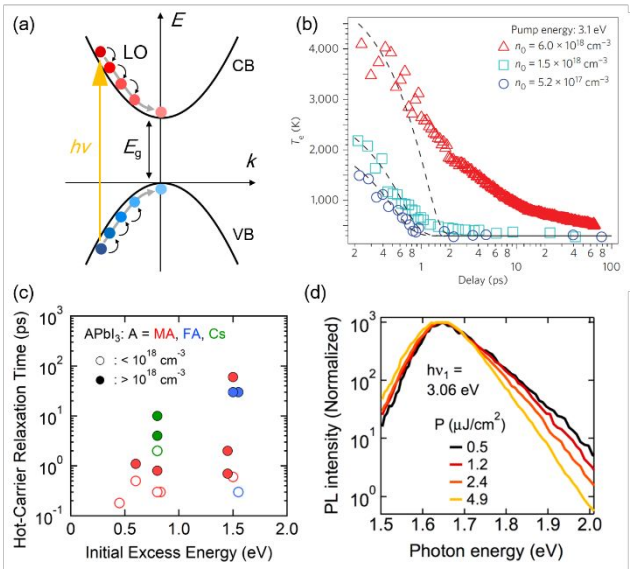

Fig. 6 (a) Schematic illustration of hot-carrier cooling in a semiconductor. Photoexcited carriers with high excess energies relax to the band edge by dissipating their kinetic energies via phonon emission. At the initial stage, the cooling is predominantly mediated by Fröhlich interaction and emission of long-wavelength LO phonons. CB: conduction band, VB: valence band, *hv*: photon energy, E_g: bandgap energy, *k*: wavevector. (b) Time-dependent carrier temperature in a $MAPbI_3$ thin film under different excitation fluences (corresponding to the initial carrier densities in the range from 0.52 to 6.0 $\times 10^{18}$ cm^{-3}). (c) Reported hot-carrier relaxation time as a function of the excess energy, hv - E_g, for the lead iodide perovskite thin films ($APbI_3$; A = MA, FA, and Cs). The data used to prepare this figure are taken from ref. 128, 129, and 142–144, where the transient absorption technique was employed to investigate the hot-carrier dynamics. The relaxation time shown here describes the time carriers require to cool down to 600 K. Strong and weak excitation conditions are represented by filled and open circles, respectively. (d) Excitation fluence dependence of the PL spectrum immediately after excitation of a $MAPbI_3$ thin film. These excitation fluences correspond to relatively weak fluences. Panel (b) is reprinted by permission from Springer Nature: Springer Nature, Nature Photonics, Yang et al.,[128] Copyright 2015. Panel (d) is reprinted with permission from ref. 152. Copyright 2016 American Chemical Society.

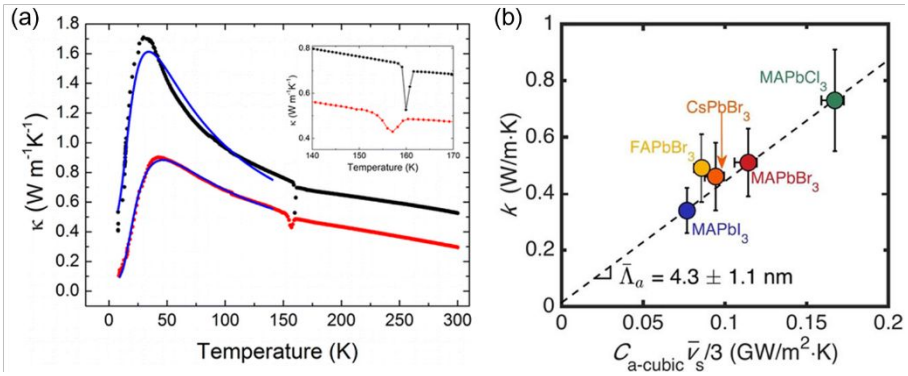

Fig. 7 (a) Thermal conductivities of a $MAPbI_3$ single crystal (black dots) and a thin film (red dots) as a function of temperature. The blue curves represent the fitting results. (b) Thermal conductivities of different halide perovskites as a function of $C_{a\text{-}cubic}\bar{v}_s/3$, where $C_{a\text{-}cubic}$ is the volumetric heat capacity of acoustic phonons based on a cubic unit cell and $\bar{v}_s$ is an average sound speed. The dashed line is a linear fit for $MAPbX_3$ and its slope corresponds to the average acoustic phonon mean free path $\bar{\Lambda}_a = 4.3 \pm 1.1$ nm. Panel (a) is reprinted with permission from ref. 30. Copyright 2014 American Chemical Society. Panel (b) is reprinted with permission from ref. 165. Copyright 2017 American Chemical Society.

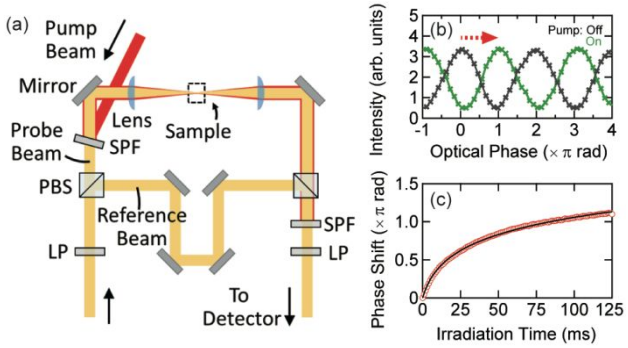

Fig. 8 (a) Schematic of the interferometer used to measure the refractive index change under photoexcitation. LP: linear polarizer, PBS: polarizing beam splitter, SPF: short-pass filter. (b) Optical phase of the probe light transmitted through a $MAPbCl_3$ single crystal without (black curve) and with (green curve) laser excitation to induce a temperature rise. A positive phase shift indicates a decrease in the refractive index due to the photo-induced heating. (c) Time evolution of the optical phase shift under photoexcitation. Panels (b) and (c) adapted from ref. 168.

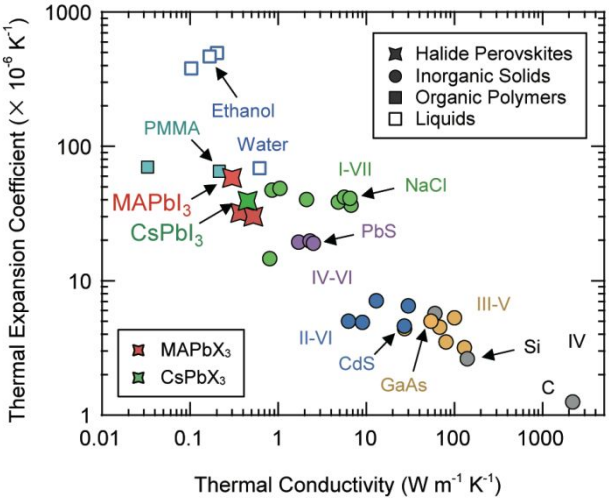

Fig. 9 Thermal expansion coefficient versus thermal conductivity for various materials. This plot is based on the data taken from ref. 170 for $MAPbX_3$, ref. 163 and 171 for $CsPbI_3$, ref. 172 for other inorganic solids, and ref. 173 for polymers and liquids.

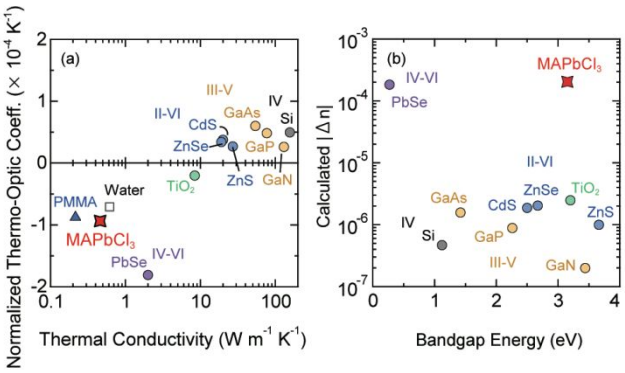

Fig. 10 (a) The normalized thermo-optic coefficients, $(1/n)(dn/dT)$, plotted as a function of thermal conductivity for various materials. (b) Calculated absolute values of the refractive-index change that occurs due to a photo-induced temperature rise for various semiconductors, plotted against the bandgap energy. Obviously, $MAPbCl_3$ exhibits a unique behavior. For the calculation we assumed an absorbed power of 20 mW and a heat conversion efficiency of unity for all materials. Adapted from ref. 168.

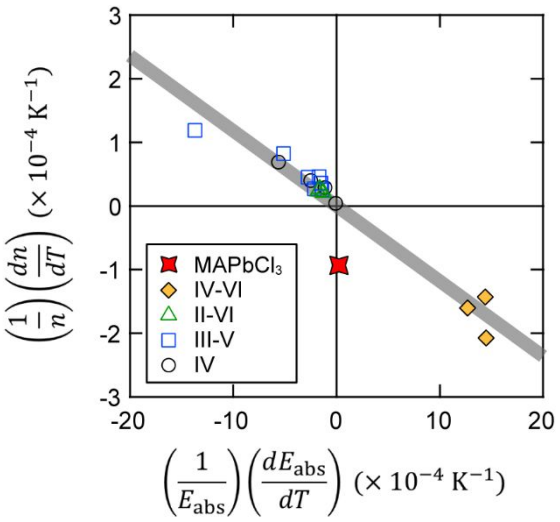

Fig. 11 Correlation between the normalized thermo-optic coefficient and the thermal shift of the absorption edge for various semiconductors. Most semiconductors lie on the gray linear line, while the halide perovskite exhibits a unique behavior. Adapted from ref. 183. Copyright 2020 The Authors published by the American Physical Society under the Creative Commons Attribution 4.0 International license.

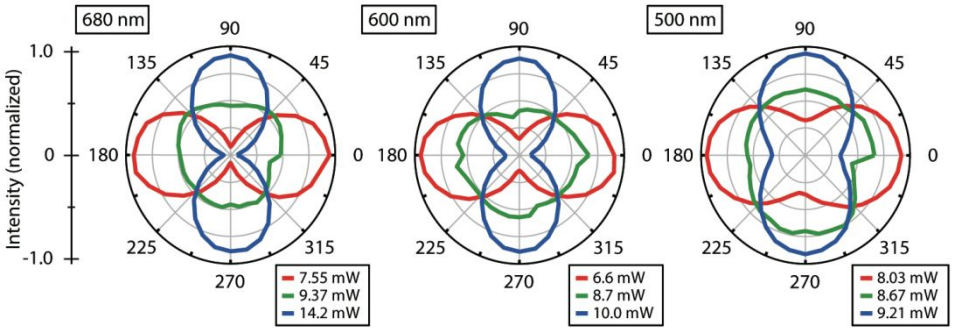

Fig. 12 Application of $MAPbCl_3$ as a thermo-optic modulator to control the polarization of visible light. Each graph plots the polarization of an optical beam that is obtained by interference between a reference beam and a beam that has passed through a $MAPbCl_3$ crystal. By changing the pump beam power incident on the $MAPbCl_3$ crystal as indicated, the optical phase of the light transmitted the crystal is controlled. This enables the precise manipulation of the relative phase difference between the two light beams and the polarization of the interfered light can be variably controlled. The wide bandgap of $MAPbCl_3$ facilitates the thermo-optic modulation in almost the entire visible wavelength region as shown with the three graphs. Reproduced from ref. 168.